Upper plate stressing and seismicity in the subduction earthquake cycle

M. A. J. Taylor, R. Dmowska, and J. R. Rice

Division of Engineering and Applied Sciences and Department of Earth and Planetary Sciences, Harvard University
Cambridge, Massachusetts

Abstract. We investigate upper plate stressing during the earthquake cycle in a subduction segment, using three-dimensional (3-D) elastic models to address the effects of strongly heterogeneous coupling along strike of the interplate interface. We show how heterogeneity controls the locations and mechanisms of seismicity in the upper plate. Oblique subduction segments, two from the Aleutians (Andreanof Islands 1986 and Rat Islands 1965) and one from Indonesia (Biak 1996) are studied. All examples of upper plate seismicity from the Aleutians represent events occurring toward the beginning of a new cycle, while in Biak, Indonesia, the examined events occur both toward the end of one cycle and the beginning of the next. In the majority of cases studied, the location and mode of the upper plate seismicity are consistent with space- and time-dependent stressing as predicted by modeling. This confirms earlier observations that seismicity in the vicinity of large/great subduction earthquakes (toward the outer rise, at intermediate depth, and now in the upper plate) depends, in an interpretable manner, on the stage in the earthquake cycle as well as on distribution of coupling along the interplate interface.

1. Introduction

Studies of seismicity near subduction margins, in the outer rise as well as at intermediate depth [*Christensen and Ruff*, 1983, 1988; *Astiz et al.*, 1988; *Dmowska et al.*, 1988; *Lay et al.*, 1989], provide evidence that there is time dependence of the style of seismicity in large regions adjacent to a strongly coupled thrust interface. In the present study we document and interpret such effects in the upper plate.

Association of regional seismicity with a major underthrusting event is most evident for the seismicity of the outer rise (including outer slope trench). Global surveys [*Astiz et al.*, 1988; *Lay et al.*, 1989] show that outer rise earthquakes with tensional normal faulting occur abundantly over an extended period after the thrust event (most happening within 10 to 20 years), whereas such events are rare or absent as the cycle matures, at which time the less frequent compressional outer rise events may occur. Such response is readily explained [*Dmowska and Lovison*, 1988; *Dmowska et al.*, 1996a; *Taylor et al.*, 1996] when we consider that the outer rise and outer slope trench is loaded by a bending stress distribution, whose propensity to cause seismicity is modulated by small extensional or compressional stress changes associated with the thrust earthquake cycle.

Further, *Dmowska and Lovison* [1992] studied the seismic response of outer rise zones in the regions of the Valparaiso (Chile) 1985, Alaska 1964, and Rat Islands (Aleutians) 1965 earthquakes. They found that the seismicity tended to cluster along strike of the subducting margin in association with known asperities (i.e., regions of highest moment release) inferred by others through modeling seismic radiation from the underthrusting events. Modeling of outer rise stress changes

when large, strong heterogeneities were distributed along strike in the seismogenic zone [*Dmowska et al.*, 1996a] gave an explanation of this clustering. This included the way that active zones in the outer rise, in the time following the thrust event, are systematically offset relative to asperity locations in regions of strongly oblique subduction as for the Rat Islands 1965 zone.

Earthquake cycle effects are also present, if less marked, in the seismicity of the slab at intermediate depth [*Astiz et al.*, 1988; *Lay et al.*, 1989], in a way that is approximately consistent with what is expected from superposition of stress fluctuations in the earthquake cycle on a time-averaged stress state dominated by slab pull [*Taylor et al.*, 1996]. *Dmowska and Lovison* [1992] showed that such intermediate depth seismicity also clustered along strike in association with asperities, but for strongly oblique convergence like for Rat Islands 1965, the clustering is offset along strike to the opposite side of the asperity from the offset in the outer rise.

In the work reported here, we examine such earthquake cycle, asperity, and obliquity effects in the upper plate. This is done through studies of seismicity in the regions of the Andreanof Islands 1986 and Rat Islands 1965 subduction events in the Aleutians and of the Biak, Irian Jaya, Indonesia 1996 subduction event. We estimate the Coulomb measure of stress change in the upper plate associated with strongly heterogeneous (asperity containing) modes of slip on the subduction interface for which stress changes are calculated from three-dimensional (3-D) models. We use such stress changes to rationalize the upper plate seismicity.

We find that regions in the upper plate which show earthquakes in the period of days to a few years after the thrust event are those which underwent an increase of Coulomb stress. That seismicity is located well outside what would normally be called the aftershock zone. In cases of tectonically active areas for which the Coulomb stress decreases, such postevent seismicity is not present, illustrating the "stress shadow" concept. This manner of

interpreting seismicity has been very successful in continental regions, particularly in association with events along the San Andreas fault system [e.g., *Harris and Simpson*, 1992; *Jaume and Sykes*, 1992; *Stein et al.*, 1992; *Reasenberg and Simpson*, 1992; *Simpson and Reasenberg*, 1994; *King et al.*, 1994; *Harris et al.*, 1995; *Harris and Simpson*, 1996]. Moreover, stress shadows from the great 1906 [*Simpson and Reasenberg*, 1994; *Harris and Simpson*, this issue] and 1857 [*Harris and Simpson*, 1996; *Deng and Sykes*, 1997] events have convincingly been argued to have masked the actual seismic hazard of tectonically active areas for many years.

2. Examples of Upper Plate Seismicity at Convergent Margins

We present three specific cases of upper plate seismicity associated with the subduction earthquake cycle.

2.1. Andreanof Islands, Aleutians

The May 7, 1986 (M_W = 8.0), Andreanof Islands earthquake ruptured an ~280 km stretch of an oblique segment of the central Aleutians (Figure 1 [after *Ekström and Engdahl*, 1989] approximate boundaries of the aftershock zone from *Engdahl et al.* [1989]), where the estimated plate motion is 82 cm/yr. (This and subsequent plate motions quoted are from the RM2

model [*Minster and Jordan*, 1978].) It was followed in the first 1.5 months by a series of shallow upper plate earthquakes close to Atka Island, of which the largest are shown in the right corner of Figure 1, all with strike-slip mechanisms [*Ekström and Engdahl*, 1989]. The five largest events range from M_W = 5.3 to M_W = 6.5 and are consistent with right-lateral motion on arc-parallel fault planes. *Ekström and Engdahl* [1989] interpret these events as occurring along a weak arc-parallel strike-slip shear zone in the upper plate, near the volcanic line, and accommodating the strike-slip part of the oblique subduction (plate convergence direction shown in Figure 1).

2.2. Rat Islands, Aleutians:

The February 4, 1965 (M_W = 8.7), Rat Islands earthquake ruptured a 600-km segment along the western end of the Aleutian Islands, where subduction is more oblique than in the Andreanof Islands segment with an estimated plate convergence rate of 86 cm/yr. The map view of the first-order asperity distribution from *Beck and Christensen* [1991] is shown in Figure 2, together with the aftershock zone (dashed line). On July 4, 1966, a shallow (depth 13 km) strike-slip m_b = 6.2 earthquake [*Stauder*, 1968b] occurred at the eastern end of the aftershock zone, the mechanism being shown in Figure 2. *Stauder* [1968b] interpreted that earthquake as left-lateral on a N-S trending fault, transverse to the structure of the island arc, in a place perhaps separating the Andreanof Islands and
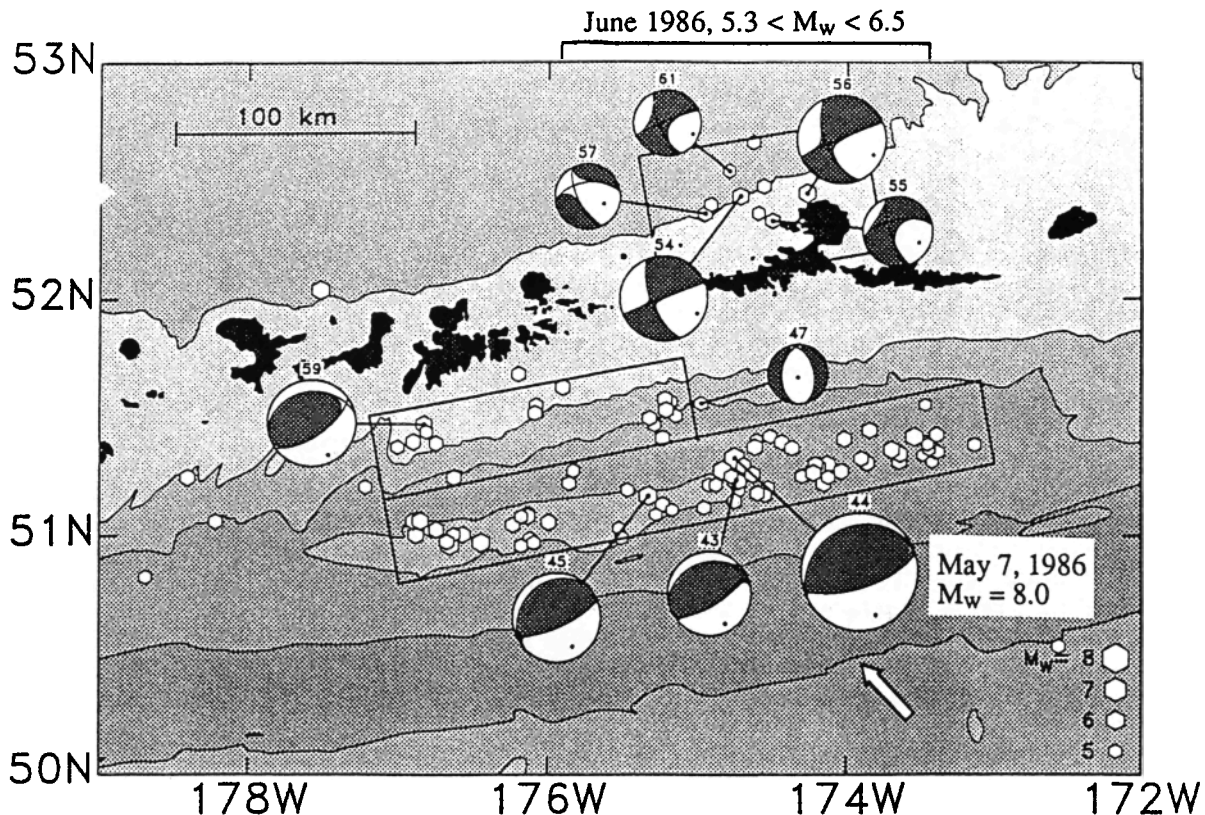

Figure 1. Back arc strike-slip activity along the Andreanof Islands section of the Alaskan/Aleutian trench following the May 7, 1986, M_W = 8.0 earthquake [from *Ekström and Engdahl*, 1989]. Approximate boundaries of the aftershock zone from *Engdahl et al.* [1989].
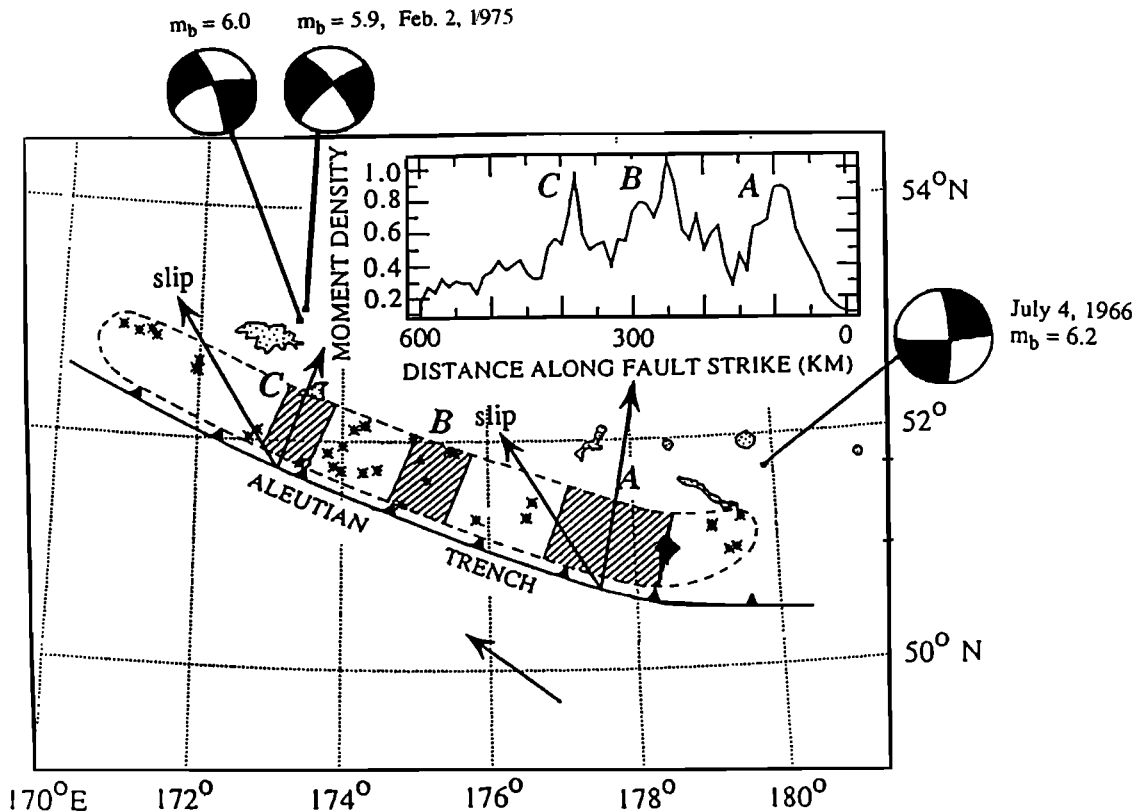
Figure 2. Strike-slip seismicity in the Rat Islands, Aleutians: Map view of asperity distribution of the Rat Islands M_w = 8.7 earthquake of February 4, 1965, from *Beck and Christensen* [1991]. Aftershock zone shown with dashed line. Mechanism of July 4, 1996, aftershock from *Stauder* [1968b] and of February 2, 1975 doublet from *Newberry et al.* [1986].

Rat Islands tectonic blocks. Figure 2 also shows two other strike-slip events (mechanisms from *Newberry et al.* [1986]), close to Near Island, north of the westernmost asperity of the 1965 event, forming a doublet of m_b 5.9 and 6.0 of February 2, 1975. This doublet was interpreted as right-lateral strike-slip motion along a northwesterly fault plane [*Cormier*, 1975b], as an extension of strike-slip faulting described by *Cormier* [1975a] in the Komandorsky Islands. *Newberry et al.* [1986] prefer to choose the northeast trending nodal plane for these earthquakes, noting that Agattu Canyon to the south of Attu Island and major faults on Attu Island itself are aligned with the trend of this nodal plane. Agattu Canyon has been interpreted as the surface expression of the boundary between two tectonic blocks of the Aleutian Arc, at least as far north as the 100-m bathymetric contour. Choice of the northeast striking nodal plane as fault plane for these events would suggest that this boundary may extend north of Attu Island.

2.3. Irian Jaya, Indonesia

The February 17, 1996 (M_w = 8.2), Biak earthquake ruptured at least 270 km along the New Guinea trench, the event being a thrust in a zone of very oblique subduction with estimated relative plate motion of 13 cm/yr. A tectonic map of Irian Jaya with the New Guinea Trench in the upper right hand corner is shown in Figure 3 [from *Puntodewo et al.*, 1994]. The map includes Biak Island, most devastated by the earthquake. As

for the other regions discussed, in the Biak area there is a discrepancy between the plate motion, very oblique to the New Guinea Trench, and earthquake slip vectors (short arrow), closer to a direction perpendicular to the trench (but still oblique). This is illustrated in Figure 3 by a dashed box next to Biak including mechanisms of earthquakes from that area, with a sum mechanism shown outside the box. The long arrows show expected motion of the Pacific plate relative to Australia, while the short arrows show the slip vector azimuth derived from summing moment tensors of earthquakes within the box [*Puntodewo et al.*, 1994]. The main event was followed by a number of events in the upper plate, the two largest of which were the M_w 6.4 (February 18) and 6.5 (February 17) events that occurred SW of the mainshock within 2 days. The mainshock was preceded by a series of events from 1979 (probably triggered by a M_w = 7.5, September 12, 1979, Yapen earthquake, close by to the southwest), in similar (but not coincident) positions to the postmainshock seismicity. All of these events are left-lateral strike-slip (or with mechanisms close to that), and together they form an approximately linear feature parallel to the main rupture, located to the SW. All mechanisms are shown in Figure 4, including the main event and two early aftershocks. For clarity, earthquakes before the main event have mechanisms shown in the top part of the figure; events after the main event are shown in the middle and bottom parts of the figure. Also, Figure 4 has been reoriented, with north pointing downward, to make later comparisons between the three cases simpler.
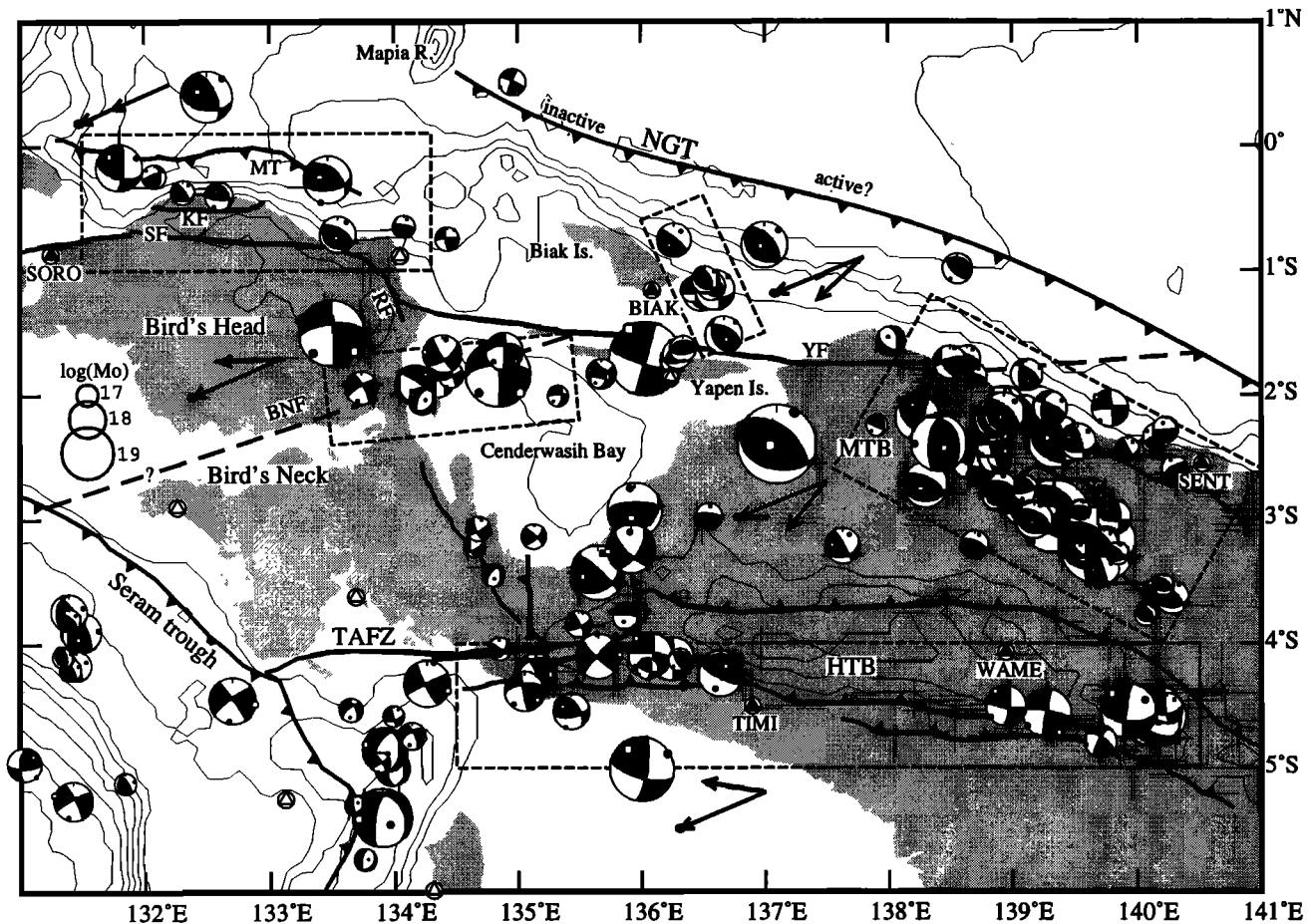
Figure 3. Tectonic map of Irian Jaya showing fault plane solutions, faults (solid lines), and inferred faults (dashed lines). Long arrows near enclosed regions show expected motion of Pacific relative to Australia, and the short arrows show the slip vector azimuths from summing moment tensors of all earthquakes in boxes. From *Puntodewo et al.* [1994].

3. Calculation of Coulomb Shear Stress

In order to interpret the back arc seismicity in each of the above examples, we adopt the concept of Coulomb shear stress. This concept has already been developed in connection with seismicity along faults of the San Andreas system [e.g., *Harris and Simpson*, 1992; *Jaume and Sykes*, 1992; *Stein et al.*, 1992; *Reasenberg and Simpson*, 1992; *Simpson and Reasenberg*, 1994; *King et al.*, 1994; *Harris et al.*, 1995; *Harris and Simpson*, 1996] and has proven valuable in understanding how stress changes from an earthquake induce (or retard) seismicity in adjacent regions. The idea of relating Coulomb stress changes to aftershock locations seems to have emerged in the work of *Stein and Lisowski* [1983] and *Rybicki et al.* [1985], although the concept that such combination of shear and effective normal stress was appropriate to understanding faulting was in use earlier [e.g., *Hubbert and Rubey*, 1959; *Rayleigh et al.*, 1972]. Further, associations between shear stress change due to earthquakes and aftershock locations were suggested by *Chinnery* [1966a, b], and *Rybicki* [1970, 1973], and effects of stress changes of major earthquakes on future large events were discussed by *Smith and Van de Lindt* [1969].

Here we extend the application of Coulomb stress to upper plate seismicity in the vicinity of subduction zones. For a planar fault with unit normal n, and unit vector in the slip direction s, the change in Coulomb shear stress, $\Delta\sigma_{ns}^c$ is defined by

$$\Delta\sigma_{ns}^c = \Delta\sigma_{ns} + f\Delta\sigma_{nn} \qquad (1)$$

where f is the friction coefficient and $\Delta\sigma$ is the change in the stress tensor. The increases or decreases in Coulomb shear stress are considered to be superimposed on the preexisting stress field in the vicinity of the subduction zone and simply modulate that overall stress field, thus promoting or inhibiting seismicity accordingly. The method pursued here is to impose coseismic slip on part of the thrust interface of our three-dimensional model of a subduction zone, in a way which allows free slip elsewhere on the interface (to represent negligible stress drop there), and to calculate the coseismic static stress changes that occur in the upper plate in response to slip on the interface.

4. Three Dimensional Modeling: Heterogeneous Slip Along Strike

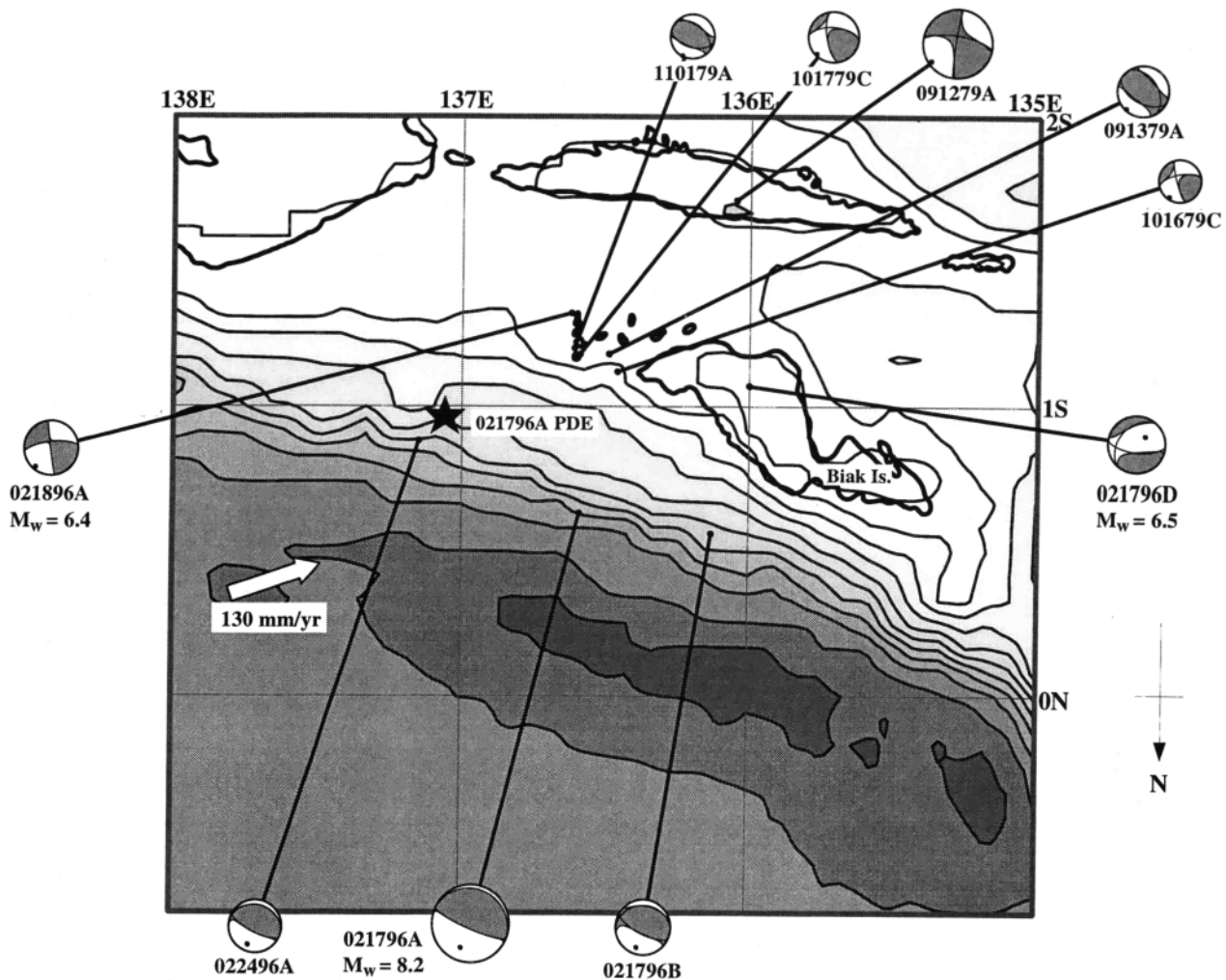For large ($M > 8$) subduction zone earthquakes, the distribution of slip along-strike is, typically, highly

Figure 4. Upper plate seismicity in Irian Jaya, Indonesia preceding and immediately following the February 17, 1996, $M_W = 8.2$ earthquake.

nonuniform with isolated asperity regions of highest slip. This is exemplified in the inversion of moment distribution for both the 1986 Andreanof Islands [*Hwang and Kanamori*, 1986, *Boyd and Nábělek*, 1988; *Houston and Engdahl*, 1989; *Das and Kostrov*, 1990; *Yoshida*, 1992] and 1965 Rat Islands [*Beck and Christensen*, 1991] (Figure 2) main events. In order to study the resulting Coulomb shear stress changes from heterogeneous slip along-strike we examine a simple 3-D model of a generic subduction zone (Figure 5) as used in *Dmowska et al.* [1996a] for calculating individually the extensional and shear stress changes due to oblique slip on asperities of various shapes and distributions. Our approach is similar here.

We incorporate an isolated region of high slip on the thrust interface (an "asperity"), indicated by the dark shading in Figure 5. The dip angle of the subducting slab, θ, the direction of obliquity from the trench-normal, ϕ, and the downdip width of the seismogenic thrust interface, W, are also shown. All of the seismogenic width slips during the simulated event, though by a spatially variable amount. We attempt to model the effect of greater slip at asperities, where there may be presumed to be a higher degree of coupling between the subducting and overriding plates, while the remainder of the

thrust interface, which is less coupled, experiences less slip in the main event. (It is assumed that the less coupled part slips aseismically or by low magnitude seismicity during the period between large thrust events.) This is simulated by applying slip of magnitude D on the asperity on the thrust interface and calculating the slip elsewhere on the seismogenic interface so as to assure that there is no net coseismic change in shear stress there during the rupture. Hence the thrust interface is modeled as "freely slipping" outside the asperity zone. The amount of slip is found to diminish rapidly from D as we move outside the asperity zone, and the slip distribution tapers to zero at the downdip edge of the seismogenic zone. Details of such modeling are given by *Dmowska et al.* [1996a]. (We have, however, noticed that contour intervals reported there for dimensionless plots of coseismic stress change were listed incorrectly; all contour intervals reported in *Dmowska et al.* [1996a] for normal stress changes should be increased by a factor of 6, and for shear stress changes by a factor of 3.) This approach may be contrasted with standard 3-D elastic dislocation modeling, in which slip is imposed, in a possibly nonuniform way, everywhere along the fault zone, without regard for the patterns of stress drop (or increase) that are thereby induced.
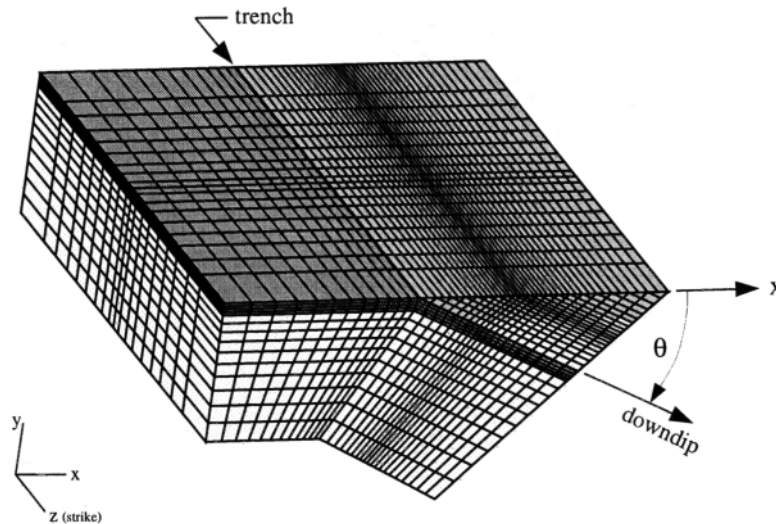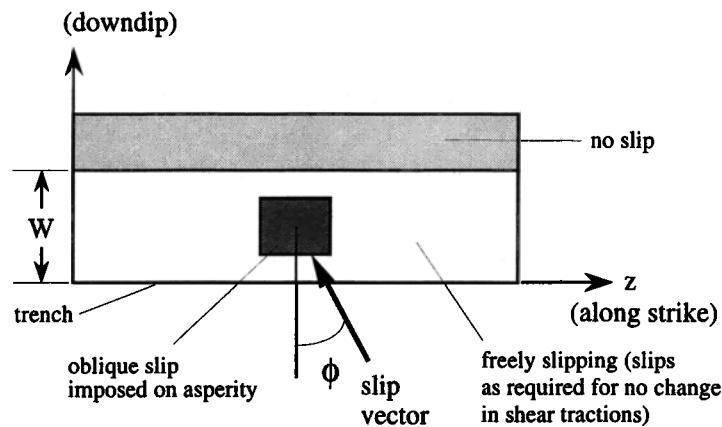
Finite Element Mesh:

trench

x

θ

downdip

y

x

Z (strike)

Thrust interface with an asperity:

(downdip)

no slip

W

z (along strike)

trench

oblique slip imposed on asperity

φ slip vector

freely slipping (slips as required for no change in shear tractions)

Figure 5. Three-dimensional finite element model with oblique slip, heterogeneous along-strike: finite element mesh and distribution of slip on thrust interface with an asperity [after *Dmowska et al.*, 1996a].

4.1. Selection of Model Parameters

In order to generate results from our models that we can compare with the locations and mechanisms of upper plate seismicity in the three regions studied here, we require approximate values for the angle of dip, θ, the angle of oblique slip from the trench-normal in the main event, ϕ, the downdip width of the thrust interface, W, and an upper plate friction coefficient, f, for each region.

1. For the Andreanof Islands, in the Aleutians, fairly good estimates for all the required parameters can be obtained from *Ekström and Engdahl* [1989] in their examination of the source parameters and seismicity surrounding the May 7, 1986, main event. In particular, Figure 5 from their paper,

showing the cross section across the Aleutian Arc with the position and nodal-planes of events on the thrust interface, allows a good estimate of θ and W. Although the thrust interface undergoes a marked increase in dip at a depth of about 30 km, it can be fairly well approximated by a plane dipping at constant angle of $\theta \approx 21°$ from base of the rupture zone right up to the trench, a distance of about 138 km (W). *Ekström and Engdahl* [1989] find that although the angle of convergence of the Pacific and North American plates is about N30°W from the trench normal, the average slip vectors for earthquakes on the thrust fault are typically 10-15° less than that (as is typical for subduction zones of oblique convergence [*Yu et al.*, 1993]), and so we examine a model where the angle of obliquity, $\phi = 18°$.

2. Parameters for the 1965 Rat Islands event are slightly harder to obtain as it occurred before the advent of the Harvard

centroid moment tensor (CMTs) and no detailed study of the geometry and velocity structure of the region has been carried out (like that of *Ekström and Engdahl* [1989] and *Engdahl et al.* [1989] for the Andreanof Islands) which would give us both estimates of the variation in angle of dip and the length of the seismogenic zone. However, an inversion of the moment distribution and an approximation of the dimensions of the rupture zone from the subsequent distribution of aftershocks has been carried out by *Beck and Christensen* [1991] (both shown in Figure 2). The source mechanism for the main event has also been inverted in a study by *Wu and Kanamori* [1973]. Assuming a constant angle of dip between the hypocenter of the 1965 event and the trench gives $\theta \approx 20°$ (from both the International Seismological Centre (ISC) data and *Wu and Kanamori* [1973]). This is also consistent with the results of *Stauder* [1968a], who finds that most of the thrust events in the aftershock series following the main event have a dip angle between 15° and 20°. Both the downdip rupture zone length and the angle of oblique slip can be estimated from the map from *Beck and Christensen* [1991] (Figure 2) which gives $W \approx 90$ km and $\phi \approx 42°$ (also consistent with the results of Wu and Kanamori).

3. The main Biak event occurred in February 1996, and at the time of writing, we have no information about any inversions for the slip distribution along the rupture plane, although we do have CMTs for the period since the event. From the CMT from the main event the dip of the rupture plane can be ascertained to be $\theta \approx 11°$, and the direction of slip on the thrust interface is around $\phi \approx -13°$ from the trench normal (ϕ measured as negative to indicate left-lateral oblique slip on the interface, opposite to that in the Aleutians). In the absence of a knowledge of the downdip extent of the rupture zone we cannot reasonably estimate W. However, the island of Biak underwent subsidence during the main February event. Its NE side subsided by 2 m, while the south and west sides dropped by < 1 m (R. McCaffrey, private communication, 1997). By examination of our 2-D modeling of uplift versus distance along the overlying plate of a generic subduction zone, [from *Taylor et al.*, 1996, Figure 13a], it is seen that vertical displacement changes are only negative (subsidence) beyond the downdip end of the rupture-zone (in a line measured from the trench and increasing out over the upper plate). Hence it seems reasonable to assume that the northern edge of the island of Biak provides an upper bound on the extent of rupture from the trench (and thus W).

Here, we do not a priori assume a value of the friction coefficient but instead employ a range of values with the stress fields computed from our model. Ideally, one could try to constrain f by comparing the results from the different values with the observed seismicity in the regions examined, but the data seldom suffice for this.

4.2. Finite Element Modeling

For subduction in the Aleutians the Pacific plate is subducting roughly SE to NW underneath the North American plate, so we impose slip on the asperity on our thrust interface in the same sense with angles of oblique slip $\phi = 18°$ and $\phi = 42°$ from the trench normal (see Figure 5), typical values based on the events in the Andreanof Islands and Rat Islands, respectively. The finite element model, which, for this

simplified geometry, has a constant angle of dip of $\theta = 20°$, was run using the code ABAQUS. Extensional and right-lateral stress changes (the relative plate motion induces right-lateral shear along arc-parallel strike-slip features in the back arc region) were obtained from the set of elements comprising the surface of the upper plate, and these were combined with a friction coefficient to calculate the right-lateral Coulomb shear stress change for the whole of that region. For the five back arc events in the Andreanof Islands the distribution of epicenters in an arc-parallel line seems to indicate that they represent right-lateral slip on arc-parallel faults, and so it is sufficient to examine right-lateral Coulomb shear stress changes on arc-parallel faults. However, for the July 4, 1966, and February 2, 1975, back arc events in the Rat Islands, it is not clear which of the two nodal planes is the actual fault plane. Hence we resolve the calculated stresses onto planes appropriate for each of the possible fault plane solutions to examine both if the position and timing of the seismicity is consistent with the coseismic stress changes form the main event, and if we can resolve which, if either, of the fault plane solutions is more consistent with those changes.

Subduction in Indonesia is in the opposite sense to that in the Aleutians, with the Pacific plate subducting left-laterally roughly ENE to WSW underneath the Australian plate. Hence in order to calculate the Coulomb shear stress distribution in the upper plate, slip is imposed on the asperity region in the finite element model in the opposite sense to that used to produce the profiles for the Aleutians, i.e., the angle of obliquity ϕ of Figure 5 is negative and chosen as $\phi = -13°$. The finite element analysis proceeds in the same way, but with a model with constant angle of dip of only 11° and changes in left-lateral Coulomb stress, $\sigma^c_{-xz} = -\sigma_{xz} + f\sigma_{xx}$, are calculated in the upper plate using a range of friction coefficients, because the relative plate motion now induces left-lateral shear along arc-parallel strike-slip features in the upper plate region. (We write the Coulomb shear stress change $\Delta\sigma^c_{ns}$ as $\Delta\sigma^c_{-xz}$ here to signify that if we choose the negative x direction for strike-slip fault normal n, then s coincides with the positive z direction.) Again, the left-lateral arc-parallel strike-slip case can be identified with direction $n = -x$ and $s = z$ in equation (1) or, equivalently, with $n = x$ and $s = -z$, with the result denoted either as σ^c_{-xz} or $\sigma^c_{x(-z)}$. We use the former notation here. The February 18 aftershock shown in the upper-plate to the east of the centroid of the main event in Figure 4 exhibits a left-lateral mechanism for an arc-parallel fault, but the preceding February 17 aftershock to the west (also shown in Figure 4) reveals a principally extensional mechanism. The direction of extension in the mechanism is ~30° anticlockwise from the direction of the trench normal. Hence, in order to investigate which regions of the upper-plate undergo extensional stress changes in a direction consistent with the February 17 aftershock being due to slip in the main event, we calculate the extensional stress changes resolved onto a plane perpendicular to a vector S30°E from the trench normal. We have also examined effects of small rotations of the n and s directions from $+x$ and $-z$, as observed for the February 18 event.

4.3. Changes in Individual Components of Stress Field: $\Delta\sigma_{xz}$, $\Delta\sigma_{xx}$, and $\Delta\sigma_{zz}$

Before examining how the Coulomb shear stress changes relate to each of the three cases, it is instructive to examine the

response of the individual components of stress change to understand how they govern the overall Coulomb stress distribution. Figure 6 shows the coseismic stress changes calculated near the surface of the upper plate for the three nonzero components of the stress field; the shear stress change, $\Delta\sigma_{xz}$ (Figure 6a), and the extensional stress changes, $\Delta\sigma_{xx}$ (Figure 6b), and $\Delta\sigma_{zz}$ (Figure 6c), from a 3-D finite element model with parameters characteristic of the Rat Islands event, i.e., $\theta = 20°$, $\phi = 42°$. This case was chosen here as the most oblique of the three cases covered, and so clearly shows the effect of obliquity on the resulting stress distributions compared to those expected form a purely dip-slip event. The

plots extend from just beyond the trench at $x = 0$ to the back of the model ($x \sim 3.25W$) and for a distance $z \sim 7W$ along-strike, with the asperity in the center of the plot at $z = 0$. The labeling on the X and Z axes should be interpreted as $X = 100(x/W)$ km and $Z = 100(z/W)$ km, respectively. The asperity, where slip D is imposed (Figure 5), extends from $0.3W$ to $0.9W$ downdip and from $z = -0.5W$ to $0.5W$ along strike, and its projection onto the surface of the upper plate is indicated by a rectangle with dashed outline. Shaded regions indicate a decrease in each stress component, and unshaded regions indicate an increase. The stress changes are plotted in terms of nondimensional parameters of the model, and the difference in
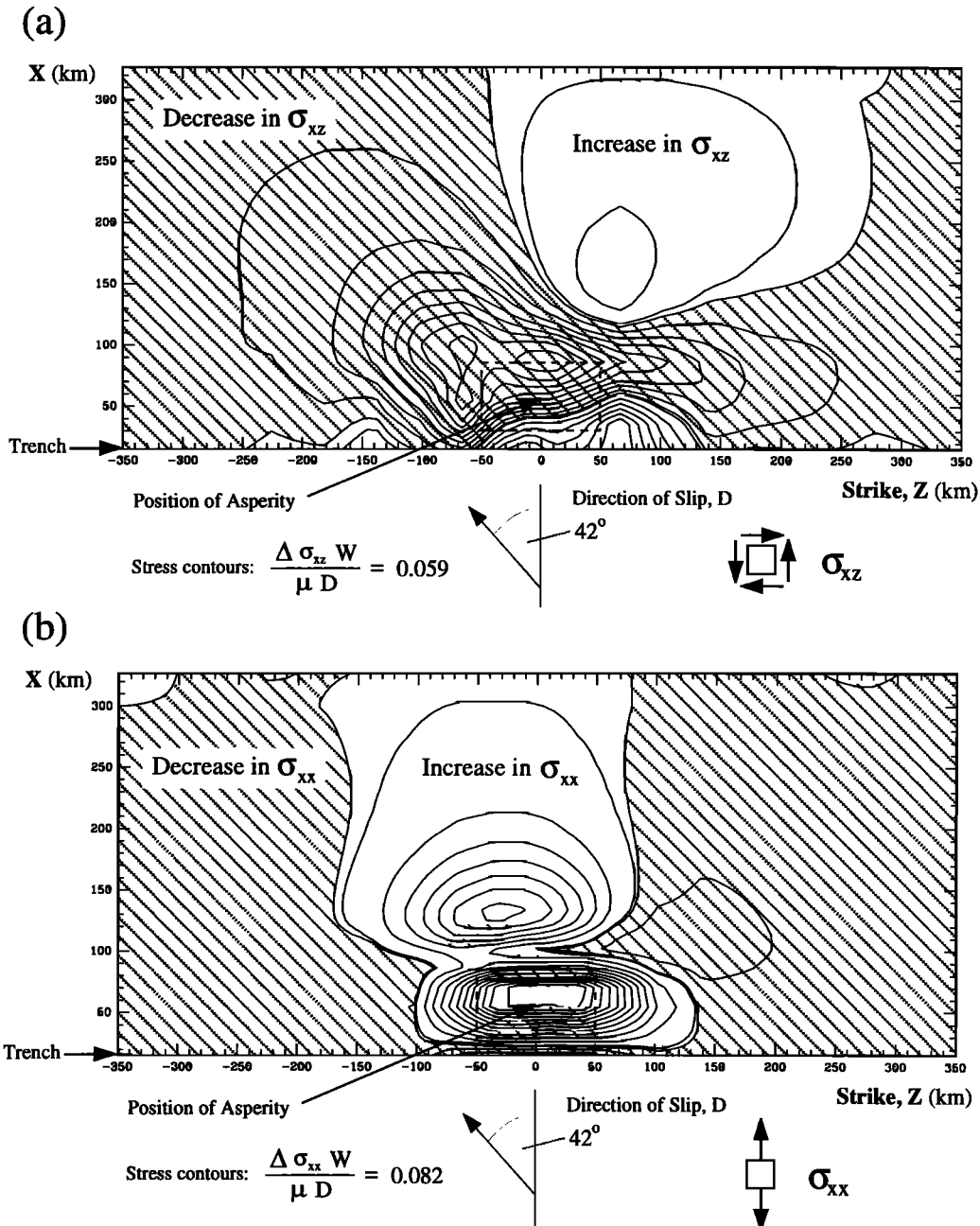
(a)

(b)

Figure 6. Coseismic changes in individual components of the stress tensor for Rat Islands-like parameters, $\theta = 20°$, $\phi = 42°$. Along-trench axis $Z = 100(z/W)$ km, and trench-perpendicular axis $X = 100(x/W)$ km. Dashed-edge box indicates projection of position of asperity onto surface. (a) Change in right-lateral shear stress on arc-parallel faults, $\Delta\sigma_{xz}$. (b) Change in trench-perpendicular normal stress, $\Delta\sigma_{xx}$. (b) Change in trench-parallel normal stress, $\Delta\sigma_{zz}$.
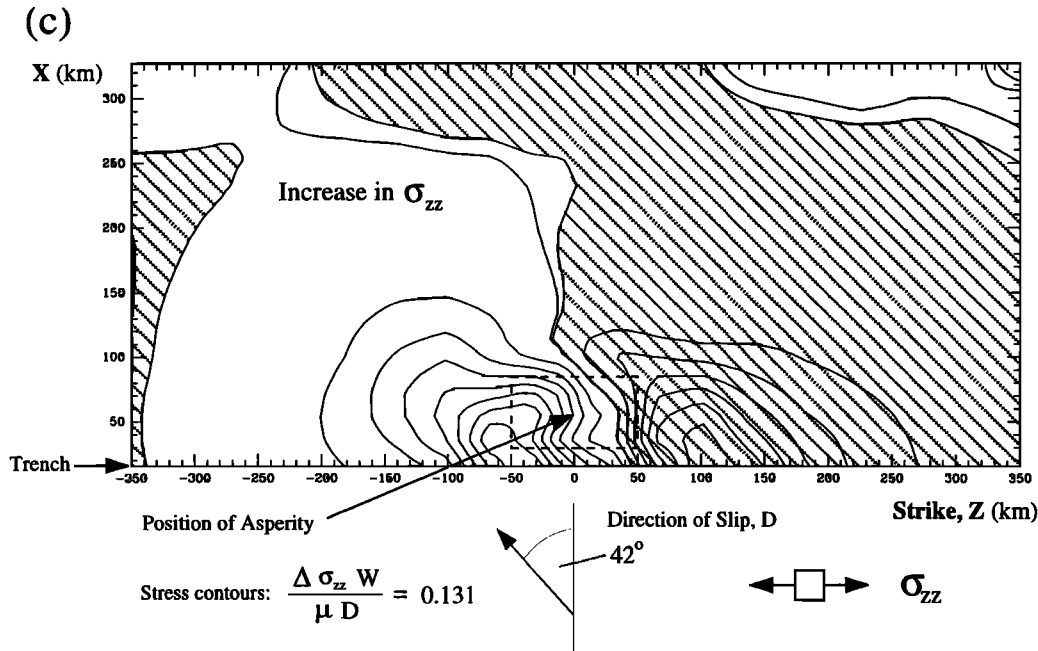
Figure 6. (continued)

stress between neighboring contours is expressed in terms of $\Delta\sigma W/\mu D$ in each figure individually. Note that the zero stress contour (that separating shaded and unshaded regions) should be treated as an additional contour, included to delineate the regions of positive and negative stress change, and near areas of zero stress change, the change in stress $\Delta\sigma W/\mu D$ is actually the difference between the first contour in the region of positive stress change and the region of negative stress change.

The pattern of coseismic $\Delta\sigma_{xz}$ shown in Figure 6a is fairly complex but has peaks of greatest stress increase at the trench, above the right-hand end of the asperity ($Z \sim 60$ km), and greatest stress decrease above the downdip end and left-hand edge of the asperity ($Z \sim 0$ and -60 km, respectively). For the region $x > W$ it separates into a broad region of increased right-lateral shear stress to the right of the asperity ($z > 0$) and increased left-lateral shear stress to the left ($z < 0$). It is important to appreciate that shear stresses are induced in the upper plate even for pure dip slip on the asperity in the 3-D model because of the edge effects from slip on a finite region of the thrust interface. The pure dip-slip case produces regions of increased (for $z > 0$) and decreased (for $z < 0$) shear stress that are symmetric in distribution, but opposite in sign, about the line $z = 0$. The introduction of oblique slip has rotated (about the y axis) the pattern in the direction of ϕ and also increased the magnitude of decrease in right-lateral shear stress, seen in Figure 6a.

The coseismic $\Delta\sigma_{xx}$ shown in Figure 6b exhibits the characteristic pattern of two peaks of increased extensional stress, one over the top of the thrust interface, and another, smaller one, in the back arc (for $x > W$). The region of increased extensional stress is concentrated in a band of width $|\Delta z| \approx 2W$ running back over the upper plate in a line oriented roughly between the direction of oblique slip, ϕ, and the trench normal with the first peak in stress centered over the asperity and the other, smaller peak, centered around $x = 3W/2$. To either side of this band the change is minimally negative.

The distribution of coseismic $\Delta\sigma_{zz}$ (Figure 6c) is broadly split into increased $\Delta\sigma_{zz}$ for $z < 0$ and decreased $\Delta\sigma_{zz}$ for $z > 0$, with the greatest increases and decreases centered over the edges of the asperity at $z = \pm W/2$. The effect of imposing oblique slip on the asperity has the same effect as seen for $\Delta\sigma_{xx}$ and causes a rotation of the distribution about the y axis by an intermediate angle, about midway from 0 to ϕ.

While Figure 6 is drawn for $\phi = 42°$, it actually lets one estimate stress changes for any value of ϕ, at least for this particular case of dip, $\theta = 20°$. That is first because the diagrams can be reinterpreted at once for ϕ reversed in sign, to $\phi = -42°$ in this case. In such transformation, $\phi \rightarrow -\phi$, the contour lines of Figures 6b and 6c have a mirror reflection about $Z = 0$, whereas those of Figure 6a have a mirror reflection followed by a reversal of sign (regions of shear stress increase become decrease and vice-versa). Then any general slip at an angle other than the $\phi = 42°$ illustrated can be resolved, by vector addition, into one slip along $\phi = 42°$ and another along $\phi = -42°$. The stress changes in response to each separate slip can be obtained from Figure 6 and its transformation when $\phi \rightarrow -\phi$ and summed to get the total stress change.

5. Comparison of 3-D Model Results to Upper Plate Seismicity

Now we examine the calculated stress changes from the 3-D finite element modeling for the specific parameters pertaining to the Andreanof Islands, Rat Islands, and Irian Jaya.

5.1. Andreanof Islands

Figure 7 shows the coseismic right-lateral Coulomb shear stress changes, for arc-parallel faults in the upper plate, for
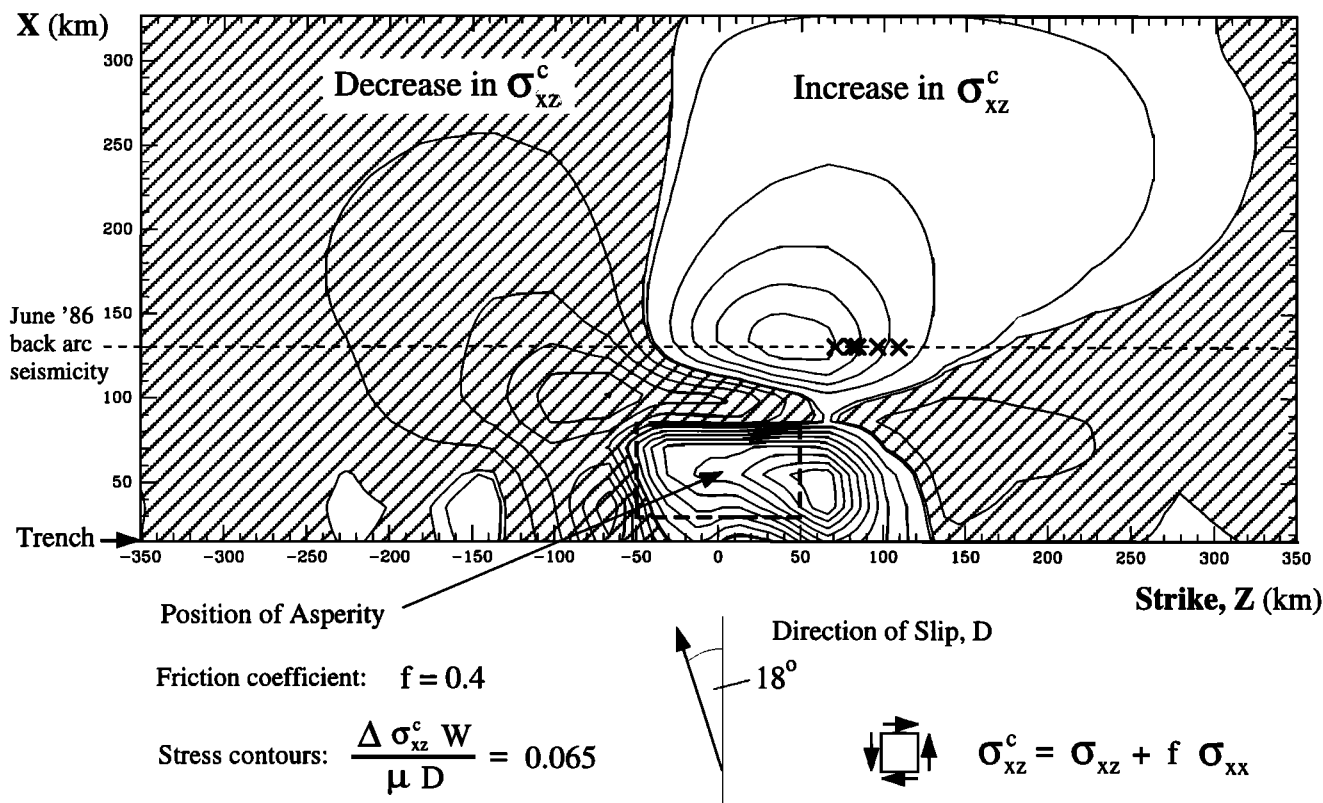
Figure 7. Coseismic change in right-lateral Coulomb shear stress $\Delta\sigma_{xz}^{c}$ on arc-parallel faults, for Andreanof Islands-like parameters, $\theta = 20°$, $\phi = 18°$, and for friction coefficient $f = 0.4$.

parameters appropriate to subduction in the Andreanof Islands. The region of the upper plate for which stresses are plotted, the axes and the shading should all be interpreted in the same way as for Figures 6a-6c. Results were obtained for a wide range of friction coefficients, f, but Figure 7 shows the stress changes for $f = 0.4$ which we show here as an midrange value for the purpose of comparison with subsequent figures for different model parameters. The difference in stress between neighboring contours is $\Delta\sigma_{xz}^{c} = 0.065\,\mu D/W$. The highest concentration of stress increase is near the trench, just to the right of the asperity, where the coseismic increase in stress, $\Delta\sigma_{xz\_max}^{c} = 0.6\,\mu D/W$, which for typical model parameters, say, $W = 100$ km, $\mu = 30$ GPa and $D = 3$m, is equivalent to $\Delta\sigma_{xz\_max}^{c} \approx 5$ bars. The general trend shows an increase in right-lateral Coulomb shear stress, consistent with seismicity with right-lateral strike-slip mechanisms on arc-parallel faults, back and to the right of the asperity and decreased stress changes, suppressing such seismicity, elsewhere. However the region of interest here is that which corresponds to distance from the trench of the June 1986 back arc strike-slip seismicity (Figure 1). For modeling the coseismic stress changes due to slip on a discrete asperity we use the inferred position of the area of highest moment release of the 1986 main event from *Das and Kostrov* [1990] which lies in the western half of the sketched aftershock zone (Figure 1) and is oriented roughly NW (between the trench normal and angle of overall plate convergence). With $W = 138$ km, measuring the corresponding distance from the trench of the June 1986 back arc seismicity from Figure 1 gives $X = 130$ km in Figure 7, and this is indicated by a dashed line. The maximum change in Coulomb shear stress at that distance from the trench is $\Delta\sigma_{xz}^{c} = 2.2 \times 10^{-3}\,\mu D\,\text{km}^{-1}$, which corresponds to about 2 bars

for the same values as above for μ and D. The five crosses ('x') in Figure 7 represent the corresponding position of the epicenters of the June 5, 1986, back arc events obtained by measuring the distance of the strike-slip seismicity along-strike in Figure 1 from the position of the asperity from the inversion by *Das and Kostrov* [1990]. All five of the events lie within the lobe of increased right-lateral Coulomb shear stress in a line spanning a range of stress increases from 1 to 2 bars (again, for the same parameters for μ and D). In other studies, calculated static stress changes of the order of 0.1 bars or greater have been deemed sufficient to be consistent with triggered seismicity following a main event, e.g., in the outer rise following a main thrust event [*Taylor et al.*, 1996] and subsequent seismicity following a large strike-slip event on the San Andreas fault [*Stein et al.*, 1992]. Here the calculated static Coulomb shear stress changes are of the order of a bar and so seem to favorably support the interpretation of the position and timing of the June 1986 back arc seismicity in the Andreanof Islands being attributed to Coulomb shear stress changes induced by nonuniform slip on the thrust interface of the May 7, 1986, main event, with highest slip (an asperity) located south and west of the subsequent back arc seismicity.

In addition to the inversion of the 1986 Andreanof Islands earthquake by *Das and Kostrov* [1990] that we use here, chosen as being the most detailed, there are several other inversions, namely by *Hwang and Kanamori* [1986], *Boyd and Nábĕlek* [1988], *Houston and Engdahl* [1989], and *Yoshida* [1992]. The inversions of Hwang and Kanamori, Boyd and Nábĕlek, Yoshida, and Das and Kostrov all show a region of highest moment release to the west of the epicenter but differ on exactly where it lies. The Das and Kostrov inversion places the main asperity the farthest west, with that of Boyd and

Nábělek about 50 km farther east (toward the epicenter, but still about 30 km west of the down dip junction in the sketched aftershock zone in Figure 1), and the main asperities from Hwang and Kanamori and Yoshida lie about midway between these. The inversion of Houston and Engdahl, however, places the main asperity just northeast of the epicenter, and directly trenchward of the June 1986 back arc events. If instead of the asperity position from Das and Kostrov [1990], we were to take the most easterly position of the asperity, from Houston and Engdahl [1989], in order to find the relative location of the five back arc strike-slip events, this would move them to the left, parallel to the Z axis in Figure 7, and center them around Z = 0. It is apparent that they would still all lie well within the zone of coseismically increased right-lateral Coulomb shear stress, and so all of the inversions are consistent with the above conclusion associating the position and timing of the back arc seismicity with the stress changes from the mainshock. Ekström and Engdahl [1989] postulate that if the region of highest moment release was directly trenchward of the back arc strike-slip events, as suggested by Houston and Engdahl [1989], then a decrease in compressive stress on the arc-parallel fault, induced by slip in the main event, could have been responsible for triggering such seismicity. We agree with this possibility but here extend it by examining patterns of Coulomb shear stress changes, thereby incorporating the effect of the shear stress changes in addition to simply the extensional stress changes. We are thereby able to show that the region of the thrust interface experiencing the highest slip in the main event that is consistent with the back arc seismicity is not restricted to lying just trenchward of the events but extends to the

southwest also. Consequently, the position of highest moment release from all of the inversions are consistent with the June 1986 strike-slip events.

5.2. Rat Islands, July 4, 1966, Event

The main difference, for the generalized parameters examined here, between the Rat Islands and Andreanof Islands events is the angle of oblique slip ϕ in the main event, around 42° for the February 1965 event compared to around 18° for the May 1986 event (Figures 1 and 2). Figure 8a shows the coseismic change in right-lateral Coulomb shear stress over the surface of the upper plate for Rat Island-like parameters. The friction coefficient used here $f = 0.4$ is to allow direct comparison with Figure 7 (for a smaller ϕ). The general features of the plot, decreased $\Delta\sigma^c_{xz}$ everywhere apart from a large peak of increased $\Delta\sigma^c_{xz}$ over and to the right of the position of the asperity and a lobe of increased $\Delta\sigma^c_{xz}$ stretching back and to the right from the trench, are extremely similar in both plots. There is also very little difference in the increment in stress change between neighboring contours, with $\Delta\sigma^c_{xz} = 0.061\,\mu D/W$ for the Rat Islands parameters. The main difference arises in the absolute value of the stress changes, the maximum stress increase (above the asperity) being about 20% less for a given slip D, and the maximum stress decrease being around 15% greater (more negative) in Figure 8a ($\phi = 42°$) than in Figure 7 ($\phi = 18°$). The stress change in the main lobe of increased Coulomb shear stress is also much greater in Figure 7, as indicated by the higher concentration of contours of the same contour spacing, then in
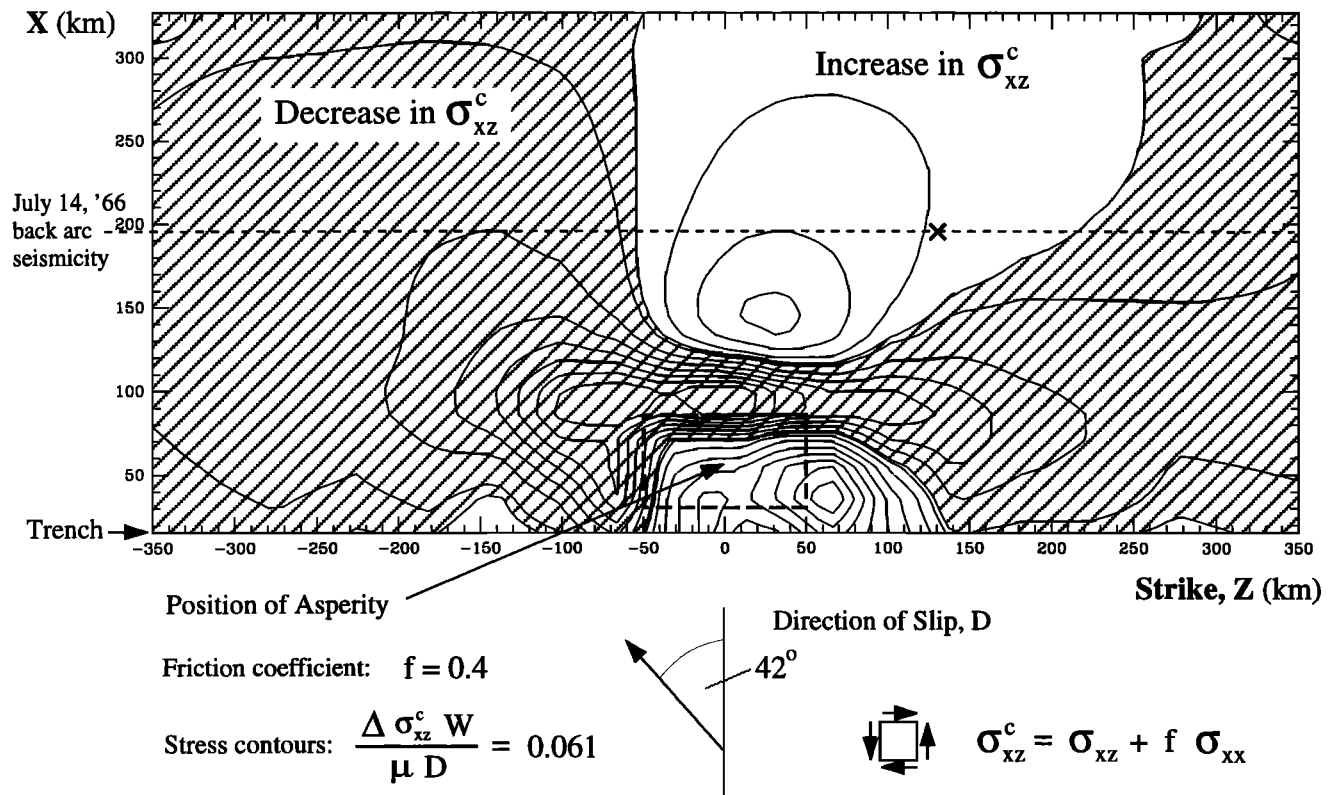

Figure 8a. Coseismic change in right-lateral Coulomb shear stress $\Delta\sigma^c_{xz}$ on arc-parallel faults, for Rat Islands-like parameters, $\theta = 20°$, $\phi = 42°$, and for $f = 0.4$.
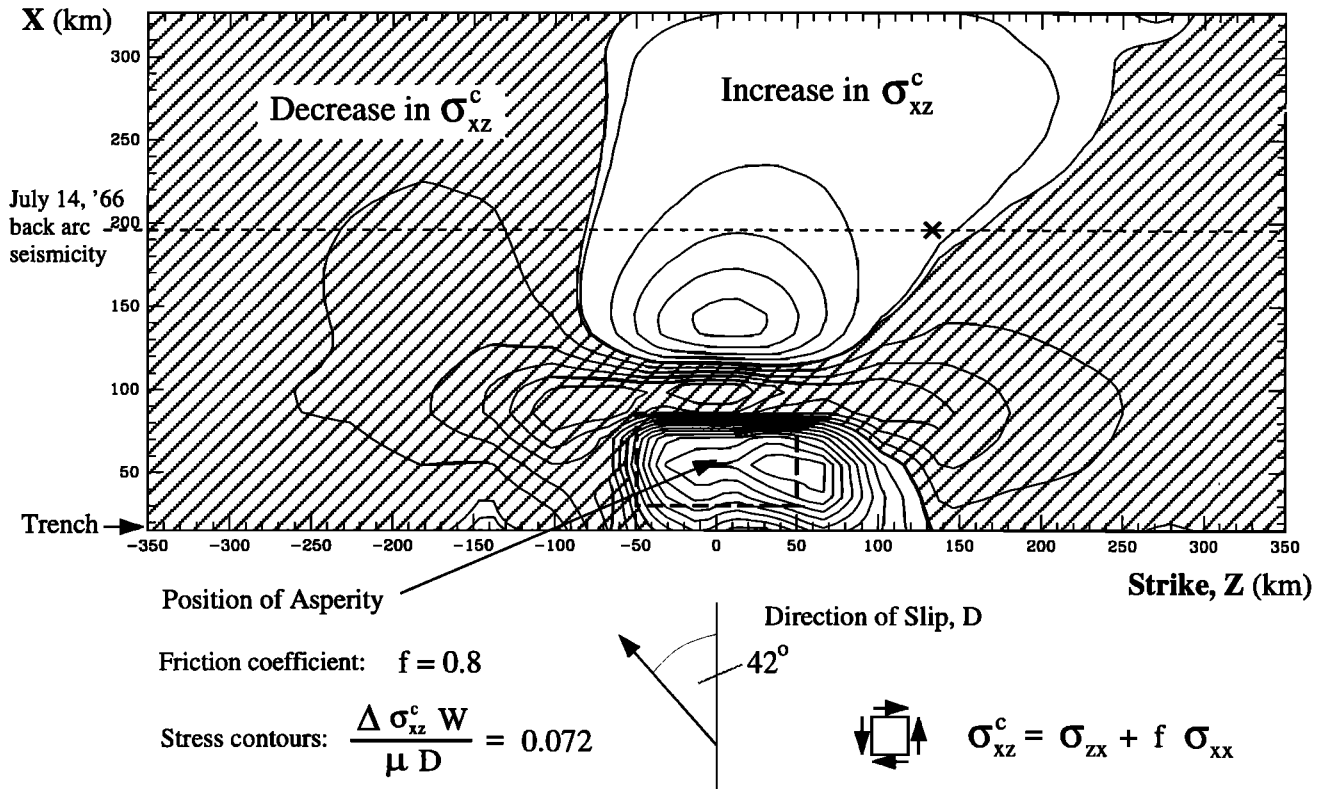
Figure 8b. Coseismic change in right-lateral Coulomb shear stress $\Delta\sigma_{xz}^c$ for parameters as in Figure 12a except for $f = 0.8$.

Figure 8a. These features are consistent with the patterns of coseismic extensional and shear stress changes induced for subduction in the sense found in the Aleutians and are plotted for parameters specific to the Rat Islands in Figure 6. The linear combination of $\Delta\sigma_{xz}$ (Figure 6a) with $\Delta\sigma_{xx}$ (Figure 6b) weighted by f produces the distribution of right-lateral Coulomb shear stress change in Figure 8a. Increasing the angle of oblique slip for the same slip D on the asperity increases the component of slip along-strike and reduces it downdip in the main event. This causes an increase in the nondimensional left-lateral shear stress change $-\Delta\sigma_{xz}$, and a decrease in the extensional stress change, $\Delta\sigma_{xx}$ over the surface of the upper plate compared to that for a smaller ϕ. Consequently, the change in right-lateral Coulomb shear stress, $\Delta\sigma_{xz}^c = \Delta\sigma_{xz} + f\Delta\sigma_{xx}$, is more negative in those regions which experienced increases in left-lateral shear stress or less positive in those experiencing increases in right-lateral shear stress. This is born out by the changes in Coulomb shear stress distribution observed between Figures 7 and 8a.

Figure 8b shows the right-lateral Coulomb shear stress change for the same Rat Islands-like model parameters as for Figure 8a but with a friction coefficient of $f = 0.8$. The general stress distribution is extremely similar to that for $f = 0.4$, and the main difference is simply the increased magnitude of the right-lateral Coulomb shear stress changes due to the extra "weighting" of the extensional stress increase by the larger friction coefficient. As a measure of this, the maximum right-lateral Coulomb shear stress increase is about 40% greater in Figure 8b than in Figure 8a, where as the maximum decrease (or, equivalently, the maximum increase in left-lateral

Coulomb shear stress) is only about 4% less in Figure 8b. This is attributable to the fact that, as outlined above, the extensional stress changes are concentrated in two main peaks which coincide with the largest changes in right- and left-lateral shear stress changes, and so they enhance the former and partially cancel the latter when combined in the right-lateral Coulomb shear stress distribution. The largest decrease in right-lateral Coulomb shear stress then lies at around $x = W$, $z = 0$, between the peaks in increased extensional stress, and so remains relatively unaltered by changes in amplitude of extensional stress and hence friction coefficient.

As with the Andreanof Islands case, we are most interested in the positions on the Coulomb shear stress plots which correspond to the subsequent back arc seismicity in the region. Figure 2 shows the known back arc strike-slip activity, one event on July 4, 1996 (with mechanism from *Stauder* [1968b]), and a doublet on February 2, 1975 (with mechanisms from *Newberry et al.* [1986]). In the Andreanof Islands case the five back arc strike-slip events of the same mechanism strung out in a roughly E-W direction strongly support the hypothesis that they are due to right-lateral slip on arc-parallel transforms and accommodate part of the slip deficit between the direction of plate convergence and slip in the main event. However, for the isolated event of July 1996 in the Rat Islands there exists ambiguity over whether it also represents right-lateral slip on an approximately trench-parallel fault, consistent with slip partitioning in a zone of oblique convergence, or instead represents left-lateral slip on an approximately trench-perpendicular fault (an interpretation favored by *Stauder* [1968b]) as part of the rotation of the most

eastern of the tectonic blocks in the Rat Islands sequence, as subsequently characterized by *Geist et al.* [1988].

Figures 8a and 8b show the Coulomb shear stress changes on arc-parallel faults, $\Delta\sigma_{xz}^{c}$. A dashed line in Figures 8a and 8b at about $x = 1.95W$ is included to indicate the relative distance from the trench of the July 14, 1996, back arc seismicity in terms of the nondimensionalized model parameters. A cross indicates the corresponding along-strike position of the epicenter measured from Figure 2. From Figures 8a, 8b, and 2 it appears that right-lateral back arc seismicity would be favored on arc-parallel faults at that distance from the trench and along-strike of the asperity from the main event. This is indeed consistent with the picture from Figure 2 where the July 14 event occurs back and to the east from the trench and of the largest of the three asperities in the moment distribution from *Beck and Christensen* [1991].

Figure 9 shows the stress distribution required to examine the alternative interpretation of the fault-plane solution, i.e. the changes in left-lateral Coulomb shear stress for arc-perpendicular faults, $\Delta\sigma_{zx}^{c}$, for the same model parameters and friction coefficient ($f = 0.4$) as Figure 8a. Apart from a narrow region near the trench for $z < 0$, the distribution of positive and negative regions of stress change is very similar in Figures 8a and 9, with the main lobe of Coulomb shear stress increase being back and to the east of the asperity (albeit for different components of the stress tensor in the two cases). A direct comparison of the stress increase at the corresponding position of the July 14 event (indicated by the cross) in the two cases reveals that in Figure 8a the increase in right-lateral Coulomb shear stress, $\Delta\sigma_{xz\_back-arc}^{c} = 0.04\mu D/W$, and in Figure 9 the increase in left-lateral Coulomb shear stress,

$\Delta\sigma_{zx\_back-arc}^{c} = 0.05\mu D/W$. Hence the Coulomb shear stress changes from our model are equally consistent with the July 14 back arc event occurring on an arc-perpendicular transform fault, as proposed by *Stauder* [1968b]. Unfortunately, then, in this instance, examination of the relevant components of Coulomb shear stress change does not allow us to distinguish between the two possible fault planes for the back arc seismicity, although it does confirm that slip on an isolated asperity in a main event would produce static Coulomb shear stress changes consistent with the position, timing and mechanism of such an back arc event.

5.3. Rat Islands, February 2, 1975, Doublet

These two events (Figure 2), a doublet, represent slip on faults that are neither arc-parallel nor arc-perpendicular. The more westerly of the two events occurred just over an hour after the other and was probably a direct result of the stress changes induced by the first event. Consequently, we examine the mechanism of only the first, more easterly of the two events for consistency with the stress changes induced by the 1965 mainshock. Measuring the angles of the two possible fault planes relative to the trench from Figure 5 of *Newberry et al.* [1986] gives the two possible interpretations of the mechanisms as either accommodating left-lateral strike-slip motion on a vertical fault oriented roughly 70° anticlockwise from the trench, or right-lateral strike-slip motion on a vertical fault oriented roughly 20° clockwise (i.e., faults striking approximately NE and NW, respectively). The stress field calculated from the finite element model used to produce
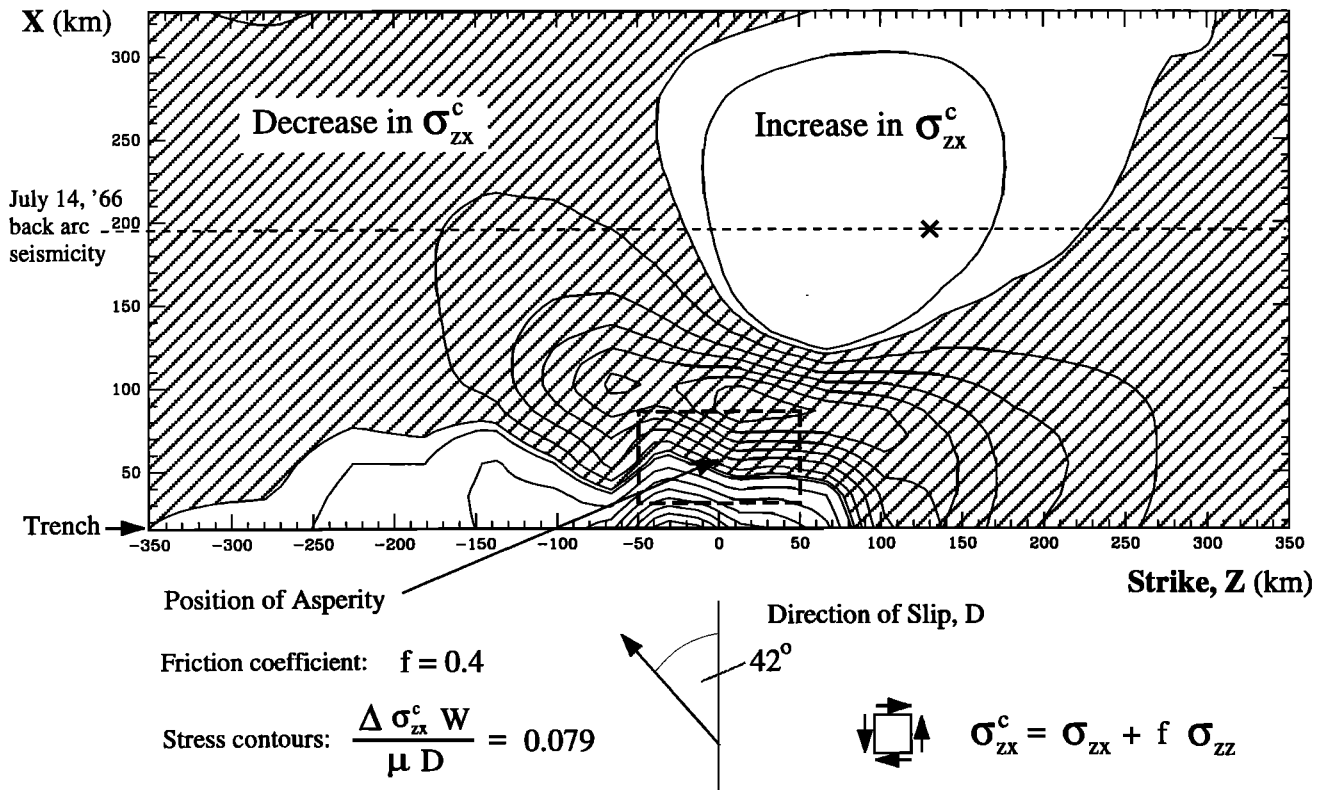

Figure 9. Coseismic change in left-lateral Coulomb shear stress $\Delta\sigma_{zx}^{c}$ on arc-perpendicular faults, for Rat Islands-like parameters, $\theta = 20°$, $\phi = 42°$, and for $f = 0.4$.

the Rat Islands-like parameter contour plots in Figures 8 and 9 for arc-parallel and arc-perpendicular faults can be resolved onto a fault of any orientation for slip in any direction on that fault by specifying a normal n and slip direction s in equation (1). Figure 10 shows the coseismic change in left-lateral Coulomb shear stress for vertical faults with n oriented 70° (measured positive in the same sense as ϕ) from the trench normal and s in the plane of the fault, as indicated in the bottom right of Figure 10, and Figure 11a shows the coseismic change in right-lateral Coulomb shear stress for vertical faults with n oriented at −20° from the trench normal, and s in the fault plane (in the opposite sense to Figure 10), again as indicated by the schematic drawing in the bottom right. Figures 11a and 11b are plotted for $f = 0.4$ as a representative midrange value of the friction coefficient. The distance back from the trench of the epicenters of the February 2 back arc seismicity from Figure 2 is indicated on the plots by a dashed line at $X \approx 160$ km (using a value of $W = 90$ km). We interpret the Coulomb shear stress changes at the position along-strike of the February 2 seismicity to be due to slip on the third (and smallest) of the three asperities indicated in Figure 2 (labeled C in the moment inversion), and the corresponding along-strike distance from the center of the asperity is indicated by a cross (using the same value of W as the scaling parameter). Figure 10 shows that the coseismic change in right-lateral Coulomb shear stress on faults oriented at 70° from the trench decreases markedly at this position. The stress decrease at the cross is $\Delta\sigma_{ns}^c = -0.002\mu D$ km^{-1}, which for representative values of parameters, $\mu = 30$GPa and $D = 3$ m, corresponds to about 2 bars. Figure 11a shows that in the same region the coseismic change in left-lateral Coulomb shear stress on faults oriented

−20° from the trench decreases to $\Delta\sigma_{ns}^c = -0.001\mu D$ km^{-1}, which represents a decrease of about 1 bar for the same model parameters. From the coseismic stress changes it appears that Coulomb shear stress changes, with an f of 0.4, resulting from slip on the third (most westerly) asperity from the inversion of the February 4, 1965, main event in the Rat Islands would tend to suppress seismicity on either of the fault planes suggested by the February 2, 1975, back arc events.

However, the February 2 events occurred 10 years after the main event, and so the distribution of stress changes in Figures 10 and 11a would have altered somewhat in that time due to any viscoelastic relaxation of the asthenosphere and continued aseismic slip both downdip from and to either side of the asperity, which presumably remains locked between large events, and from ongoing tectonic loading. Although it is a feasible extension of our modeling to calculate the fluctuating stress field throughout an entire earthquake cycle, as done for a 2-D model (homogeneous along-strike) by *Taylor et al.* [1996] and *Zheng et al.* [1996], here we have simply calculated the coseismic stress changes. Such modeling shows that the pattern of coseismic stress change gradually reverses (positive to negative and vice versa) during the earthquake cycle, at least in the idealized case when each cycle periodically duplicates previous ones. This reversal occurs linearly with time if a purely elastic response from the model is assumed and in a nonlinear fashion if a viscoelastic, or other time-dependent response is introduced. It is likely that even 10 years represents only a relatively small fraction of the cycle time in the Rat Islands, and so the distribution of Coulomb stress changes would still be positive and negative where shown as such in Figures 10 and 11a, but the magnitude
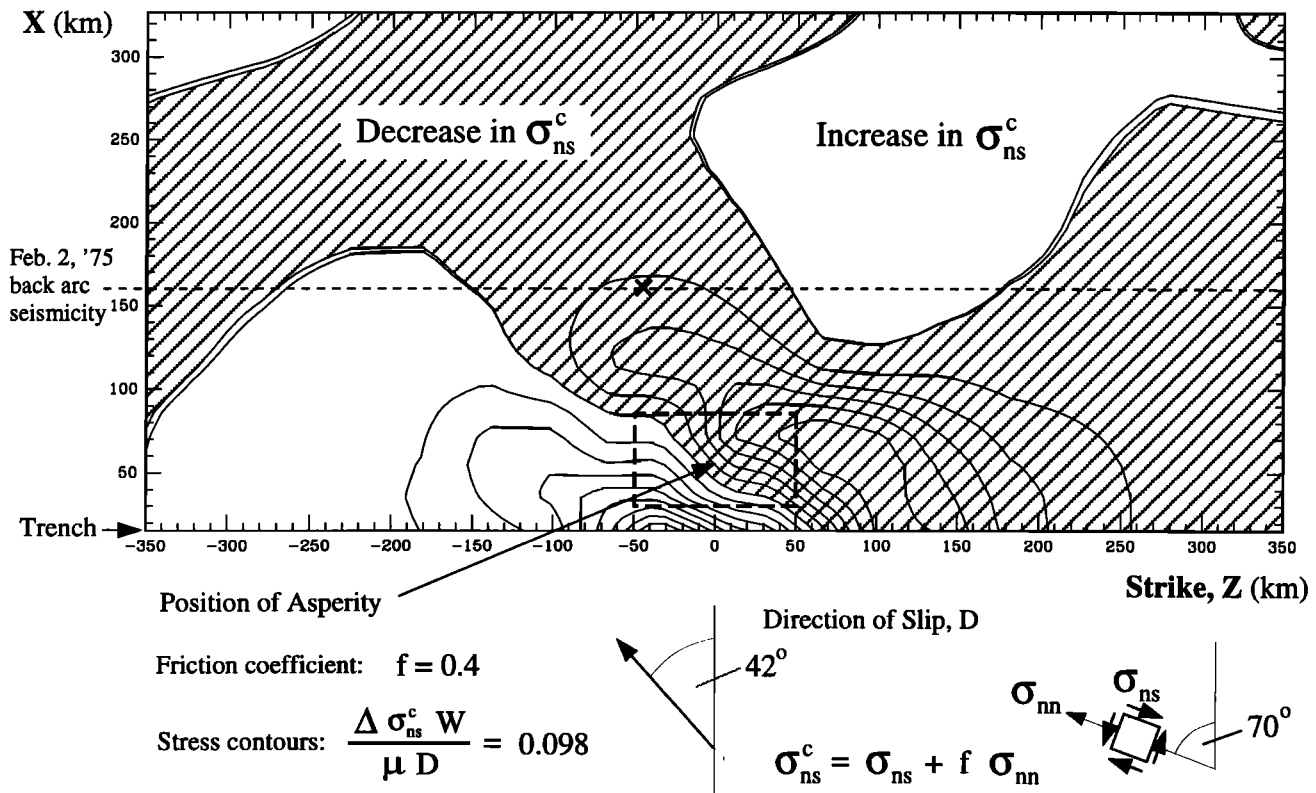

Figure 10. Coseismic change in left-lateral Coulomb shear stress $\Delta\sigma_{ns}^c$ on faults oriented at 70° anticlockwise from the trench, for Rat Islands-like parameters, $\theta = 20°$, $\phi = 42°$, and for $f = 0.4$.
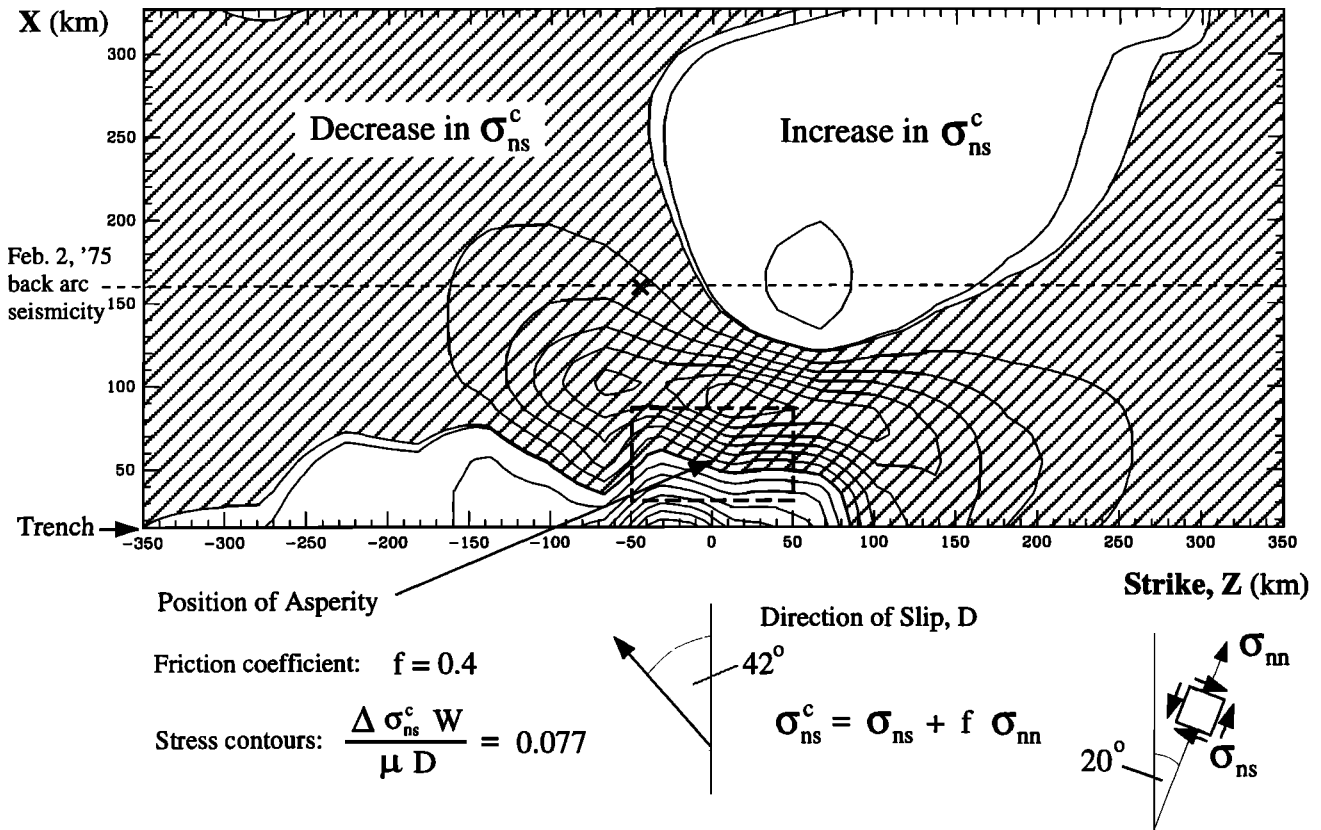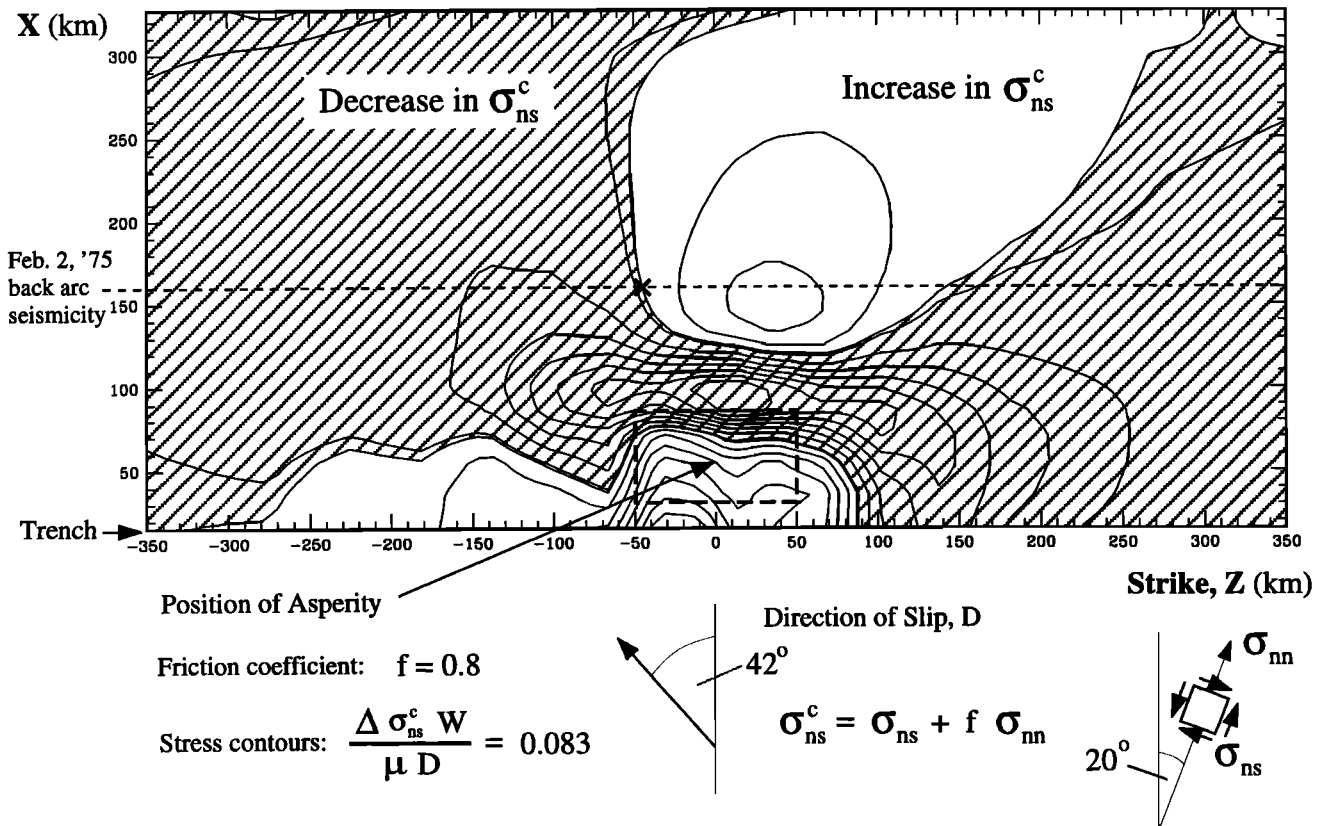
Figure 11a. Coseismic change in right-lateral Coulomb shear stress $\Delta\sigma_{ns}^c$ on faults oriented at 20° clockwise from the trench, for Rat Islands-like parameters, $\theta = 20°$, $\phi = 42°$, and for $f = 0.4$.

Figure 11b. Coseismic change in right-lateral Coulomb shear stress $\Delta\sigma_{ns}^c$ on faults oriented at 20° clockwise from the trench, for parameters as in Figure 14a except for the friction coefficient $f = 0.8$.

of the changes would be diminished from their coseismic values. Although the magnitude of the Coulomb shear stress decrease at the position of the February 2 back arc events is less for the SE-NW striking plane (in Figure 11a), even 10 years after the main event, the decrease in stress with both cases would still be a significant fraction of a bar (for typical model parameters and an $f = 0.4$). Hence it is unclear whether the background stress field could have increased sufficiently over that time to cause a net increase in Coulomb shear stress, and so we cannot rule out the possibility that the back arc seismicity was induced by stress changes from activity on other nearby faults, not from the main event.

Another consideration regarding the temporal variation in Coulomb shear stress changes is the dependence of the distribution on f. Figures 10 and 11a are both for a typical, midrange value $f = 0.4$. One possibility regarding the dependence of f on pore fluids in the fault zone which has been raised [*Simpson and Reasenberg*, 1994] is that coseismically, fluids trapped in the rock result in a low effective coefficient of friction (e.g., $f = 0.2$ or lower) because extensional normal stress change induces a change of opposite sign in pore pressure but that subsequently, as fluids drain away, the effective coefficient of friction increases (e.g., up to $f = 0.8$). Figure 11b shows the coseismic right-lateral Coulomb shear stress changes for the same (SE-NW striking) fault plane as in Figure 11a, but with $f = 0.8$. The principal differences in Figure 11b (compared to Figure 11a) are the increase in maximum stress change, both above the asperity and in the main lobe back and right from the trench (indicated by more stress contours of greater $\Delta\sigma^c_{ns}W/\mu D$) and that the main region of increased stress change has rotated slightly about the y axis in the direction of increasing ϕ. Both of these are due to the increased weighting of the extensional stress changes in the distribution. The corresponding position of the Feb. 2 back-arc seismicity (marked by a cross) for $f = 0.8$ lies just inside the region of increased stress, compared to inside a region of decreased stress for $f = 0.4$ (Figure 11a). If indeed there is a time dependence in the effective value of the coefficient of friction, the propagation of the region of increased Coulomb shear stress as f increases during the earthquake cycle could provide another mechanism for triggering of subsequent seismicity in the back arc other than simply the coseismic response to the main event. It is important to note that the position of the last, third asperity is the most poorly constrained in *Beck and Christensen's* [1991] inversion, which is reflected in the uncertainty in the relative position of the February 1975 events (cross) in Figures 11a and 11b. The critical point is therefore not that the cross falls right on the border of increased/decreased right-lateral Coulomb shear stress for an $f = 0.8$ but rather that the region of increased right-lateral Coulomb shear stress expands westward with increasing f (e.g., 0.2 to 0.8, Figures 11a and 11b, respectively).

The results shown here are all from models which use an asperity of the same downdip and along-strike dimensions, which are characterized in terms of a single parameter W. However, the inversion used by *Beck and Christensen* [1991] does not allow the determination the downdip extent of their asperities for the 1965 Rat Islands event (Figure 2). The along-strike length of the asperity in our model used to generate plots 6-13 is W. Changing this would affect the distribution and magnitude of the stress changes and so raises the question of the validity of using the same model (and width

of asperity) to interpret both the stress distribution for the July 4, 1966, back arc seismicity (Figures 8 and 9) in association with asperity A and the February 2, 1975, back arc seismicity (Figures 10, 11a, 11b) in association with asperity C. However, preliminary runs with an asperity of length $2/5$ W show that the main differences in stress distribution occur only very close to the trench and are small and that back from the trench beyond $z \sim W$ the distribution is almost identical to that for the larger asperity. In this region the magnitude of the stress changes is decreased almost uniformly by a factor of $\sim 2/3$ as a reflection of the response to the same magnitude of slip D being applied over a smaller area in the main event. However, even taking into account the uncertainty in position and size of the asperity, we cannot definitively rationalize this doublet, 10 years after the Rat Islands event, as a consequence of stress changes in the event.

5.4 Irian Jaya

For Irian Jaya, Figure 12 shows the coseismic change in left-lateral Coulomb shear stress in the upper plate on arc-parallel faults for the same range of x and z as Figures 6-10, and for $f = 0.4$. The direction of slip on the assumed asperity ($z = 0$) is indicated as $\phi = -13°$, and the contours between lines of constant stress change are shown with separation $\Delta\sigma^c_{-xz}W/\mu D = 0.136$, with decreases in stress indicated by shaded regions and increases by unshaded regions. The general features of Figure 12 closely resemble the plots of Coulomb shear stress change on arc-parallel faults due to subduction in the opposite sense (Figures 6, 7a, and 7b for the Andreanof and Rat Islands, respectively) but with the pattern of stress changes reflected about the line $z = 0$, as one would expect. The increment in stress contours is over twice that found in the plots for the Aleutians. Part of the reason is the shallower angle of obliquity, which tends to deemphasize the change in shear stress and to emphasize the change in extensional stress, thus creating higher overall changes in Coulomb shear stress, but the more dominant effect is from the shallow angle of dip in Irian Jaya ($\theta = 11°$ in the finite element model), which means the stresses resulting from slip on the thrust interface have a shorter distance in which to attenuate before reaching the surface. The lack of a seismic inversion for the Biak event at time of writing again leaves us without reliable values to fit to the parameters of the model, and so no dashed line appears in Figure 11 to indicate the position of upper plate seismicity as no definitive value is known for W, only the upper bound noted earlier. However, we would expect the upper plate events of Figure 4 to lie at least beyond the downdip end of the thrust zone, which, for the 11° dip angle used in the finite element model, corresponds to $X > 98$ km.

Figure 13 shows the extensional stresses induced by slip at $\phi = -13°$ on the asperity resolved on a plane 30° anticlockwise from the trench (orientation shown in bottom right of Figure 13). Decreases in extensional stress are shown by shaded regions and increases are shown by unshaded regions. The pattern of extensional stress change for this orientation is almost exactly opposite of that of the left-lateral Coulomb shear stress change in Figure 12, with a region of stress increase back and to the right of the asperity and decreases in stress everywhere else. Again the highest stress change is located right above the asperity, but the region we are interested in lies beyond $X \sim 98$ km.
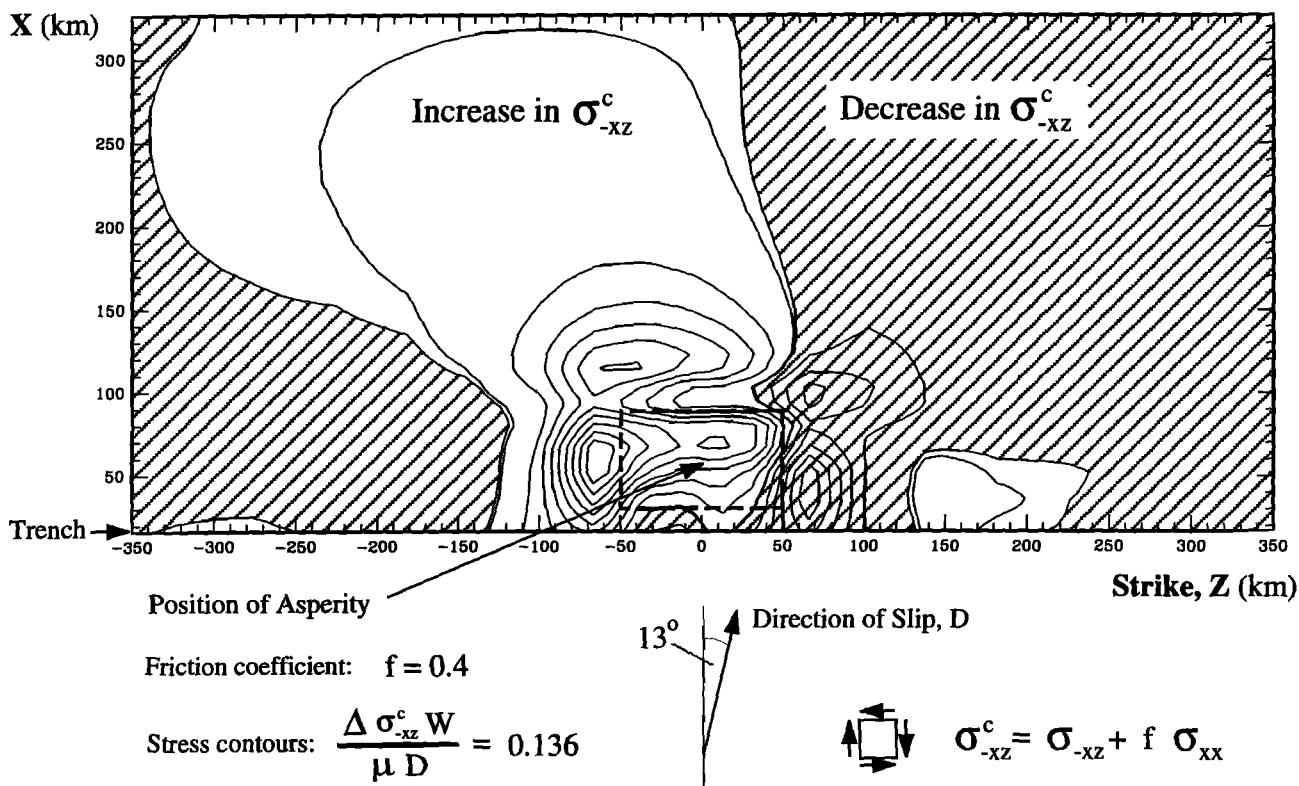
X (km)

Increase in σ^c_{-xz} Decrease in σ^c_{-xz}

Trench →

Strike, Z (km)

Position of Asperity

Friction coefficient: f = 0.4

Direction of Slip, D

13°

Stress contours: $\dfrac{\Delta\, \sigma^c_{-xz}\, W}{\mu\, D} = 0.136$

$\sigma^c_{-xz} = \sigma_{-xz} + f\, \sigma_{xx}$

Figure 12. Coseismic change in left-lateral Coulomb shear stress $\Delta\sigma_{-xz}$ on arc-parallel faults for Irian Jaya-like parameters, $\theta = 11°$, $\phi = -13°$, and for $f = 0.4$.

X (km)

Decrease in σ_{nn} Increase in σ_{nn}

Trench →

Strike, Z (km)

Position of Asperity

Direction of Slip, D

13°

Stress contours: $\dfrac{\Delta\, \sigma_{nn}\, W}{\mu\, D} = 0.189$
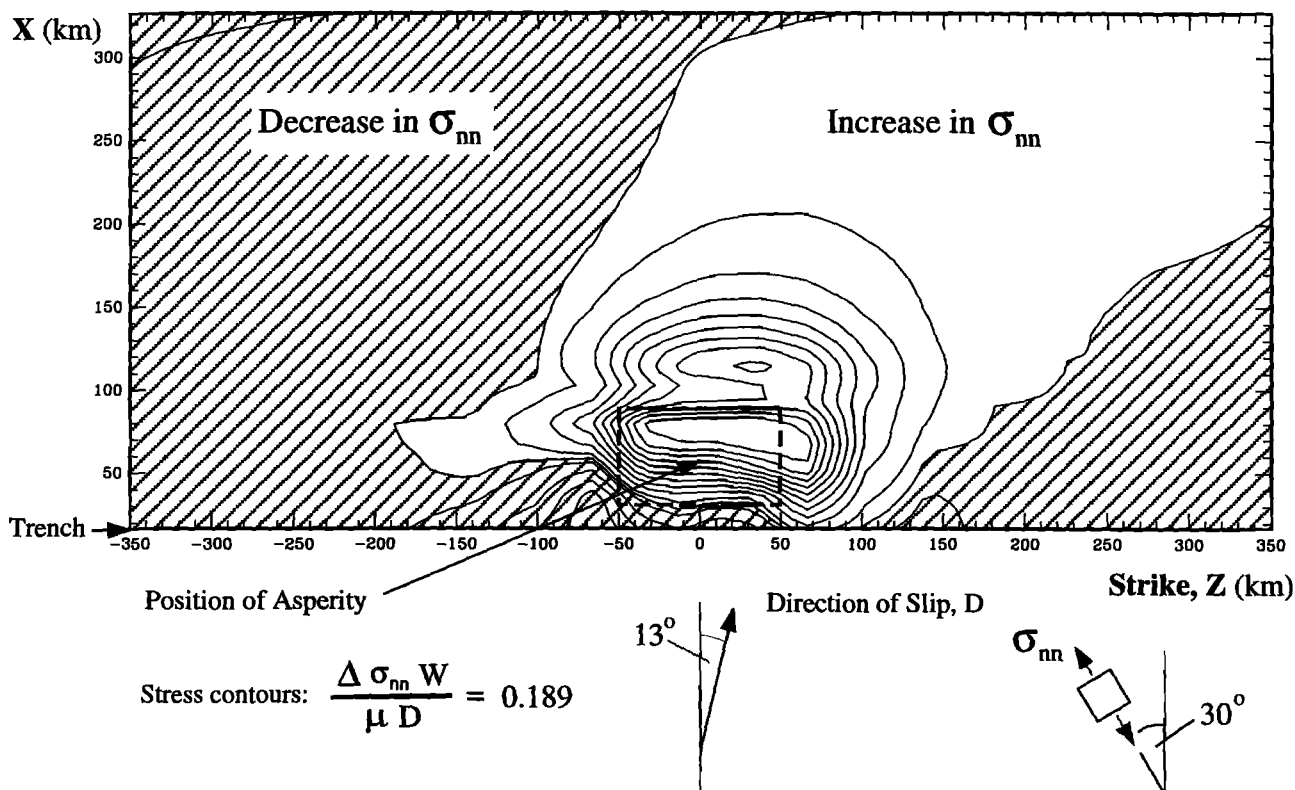
σ_{nn}

30°

Figure 13. Coseismic change in extensional normal stress $\Delta\sigma_{nn}$ on faults oriented at 30° anticlockwise from trench for Irian Jaya-like parameters, $\theta = 11°$, $\phi = -13°$.

From comparison of the positions of the two upper plate events (Figure 4) and the corresponding calculated stress change profiles from Figures 12 and 13, we can infer the approximate position of an asperity on the thrust interface which is consistent with the position, mechanisms, and timing of these events. Figure 14 shows all the seismicity in the region from the various Harvard CMT catalogs, $M > 5$, from February 17 until July 1997, which includes some of the smaller aftershocks not reported immediately (and not shown in Figure 4) and also considerable upper plate seismicity. The earthquakes have been split into three groups: (1) those with principally thrust mechanisms consistent with the orientation and shallow dip angle of the thrust interface, shown along the base of Figure 14, (2) those with primarily extensional mechanisms, shown along the right of Figure 14, and (3) those with right-lateral strike slip or right-lateral strike slip with a thrust component which are shown in the upper left of Figure 14. Most of the upper plate seismicity exhibits distinctly nondouble-couple solutions and so these divisions are fairly general, although surprisingly distinct none the less. It is apparent that the upper-plate extensional and strike-slip mechanisms 2 and 3 fall into distinct groups relative to the position of the centroid of the main event, explicitly, the extensional events to the "right" (west) and the strike-slip events to the "left" (east). This is exactly consistent with Figures 11 and 12 if slip occurred on an asperity between these

groups, and so a tentative sketch of the position of such an asperity is shown by the hatched ellipse in Figure 14 above where the thrust interface appears to be, based on the position of the centroid and aftershocks. The fact that there are 13 events which all seem to follow this pattern of stress distribution makes this explanation of an asperity location fairly compelling, and it will be of interest to examine any subsequent seismic inversions of the February 17 event, to compare the distribution of moment release from such an inversion with what we have inferred from the upper plate seismicity. The high tectonic complexity of the upper-plate in the Biak area (Figure 3) may be the reason for the abundant seismicity following and preceding the 1996 main event.

6. Discussion and Conclusions

Our study of 3-D models with strongly heterogeneous slip reveals complex distributions of both shear and extensional stress change which can be related to the edge effects of the finite region of largest slip. The distributions show a strong dependence on the various model parameters, θ, ϕ, W (Figure 5), and f. Increasing the angle of dip θ reduces the magnitude of the stress changes everywhere in the upper plate and compresses the distribution toward the trench. Increasing the slip obliquity angle ϕ increases the weighting of the shear
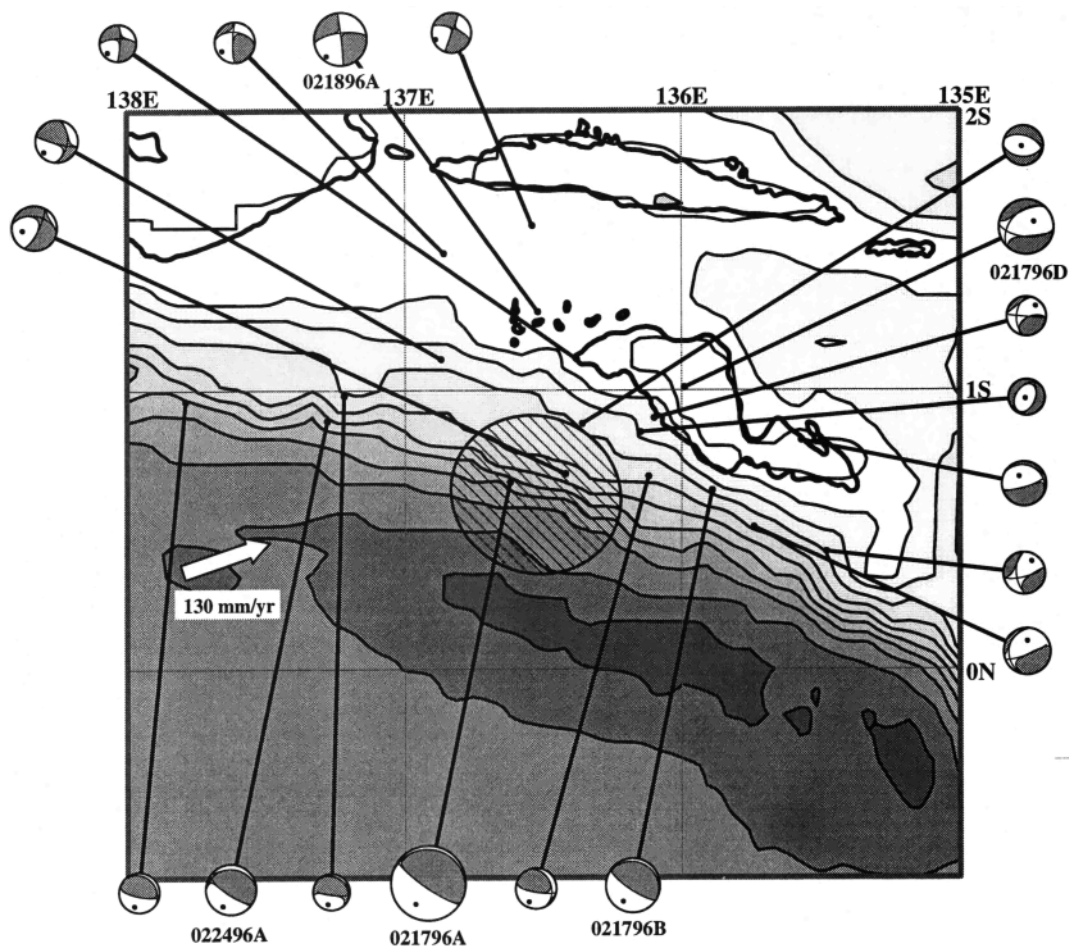

Figure 14. Back arc seismicity in Irian Jaya, Indonesia, following the February 17, 1996, $M_W = 8.2$ earthquake (February-July 1997).

stress changes over the extensional stress changes in the Coulomb shear stress change distribution, as well as increasing the angle at which the peaks in extensional stress increase are oriented over the back arc. Reducing the along-strike length of the asperity from the total interface width W has an almost negligible effect on the Coulomb shear stress distribution beyond $z > W$ and simply reduces the magnitude of the changes uniformly in that region. Increasing friction f has the opposite effect to that of increasing ϕ and increases the weighting of the changes in extensional stress over the shear stress changes.

The Coulomb shear stress distributions due to heterogeneous slip show qualitative consistency with the observations for the Aleutians and Irian Jaya. Such models predict that in presence of oblique slip directed like in the Aleutians, beyond the downdip end of the thrust interface, localized zones of right-lateral $\Delta\sigma_{xz}^c$ on arc-parallel faults are created postseismically just to one side of an asperity in the back arc region and that $\Delta\sigma_{xz}^c$ is left-lateral (discouraging activity) elsewhere (Figures 7, 8a, and 8b). We show results for $f = 0.4$ and 0.8 and for slip obliquity of 18° and 42° here, and cases that we studied with other obliquity angles and with $f = 0.0$, 0.2, or 0.6 gave similar features of localized zones of right-lateral $\Delta\sigma_{xz}^c$ to one side of an asperity and left-lateral $\Delta\sigma_{xz}^c$ elsewhere (which is good for robustness of predictions but unfortunately shows that strongly heterogeneous coupling will not provide any constraints on f). Work addressing Coulomb stress interactions in southern California [Stein et al., 1992; King et al., 1994; Harris et al., 1995; Harris and Simpson, 1996] also failed to definitively pick a best f to explain the data, and so typically 0.4 has been chosen as a representative value.

The pattern in Figure 7 is consistent with the position and timing of the postmainshock series of right-lateral strike-slip events in the Andreanof Islands (Figure 1) and the pattern in Figures 8a and 8b shows consistency with the July 1966 seismicity in the Rat Islands (Figure 2) if it occurred on an arc-parallel fault. Examination of the left-lateral Coulomb shear stress changes on arc-perpendicular faults for the Rat Islands (Figure 9) shows that these are also consistent with the position and timing of the July 1966 event. The Coulomb shear stress changes resolved onto the two possible fault planes for the February 1975 seismicity in the Rat Islands show a decrease in both cases for $f = 0.4$ (Figures 10 and 11a). However, the decrease for the SE-NW striking plane (as proposed by Cormier [1975a, b]) is less in the same region than for the alternative, and a plot using an $f = 0.8$ (perhaps justified by pore pressure relaxation given the 10 year period since the main event) actually reveals a very modest increase in Coulomb shear stress there.

For the case of upper plate seismicity following the 1996 Biak, Irian Jaya, event, we interpret all the earthquakes, premainshock and postmainshock, as accommodating the strike-slip part of the oblique subduction, with their positions in space and time (before or after the mainshock) reflecting the heterogeneous coupling along the main rupture zone, as modeled in 3-D for oblique subduction segments with asperities. Based on the spatial positions of all these earthquakes, we tentatively attempt to estimate the region of highest seismic slip (and the highest coupling) in the Biak 1996 earthquake, observing that models of strongly heterogeneous slip show that postseismically, localized zones

of left-lateral shear stress are created to one side of an asperity, whereas stresses favoring more extensional faulting are induced on the other side. This pattern is exemplified by the postmainshock February 18 and 17 events (Figure 4) and subsequent seismicity up to the present (Figure 14) provided that the asperity is located in the rupture zone between the positions of those two earthquakes.

Such a position of an asperity also seems consistent with the locations of the 1979 premainshock earthquakes, which are observed to be directly adjacent to it (Figure 4). Those were apparently induced by the September 12, 1979 ($M_W = 7.5$), earthquake on the Yapen fault. The 1979 sequence has compressional components, and the late cycle trench-perpendicular compressive stress should indeed be greatest in the upper plate, directly back of a locked asperity [Dmowska et al., 1996b]. Also, the 1979 strike-slip earthquakes of October 16 and 17 have locations (Figure 4) somewhat to the west of the abundant strike-slip activity (Figure 14) occurring after the subduction event. We may recall that the gradual stress changes during the earthquake cycle must, approximately, be the same as the coseismic stress changes, but with signs reversed. Thus the region in the upper plate under highest left-lateral Coulomb stress in 1979 should coincide with the region which underwent coseismic decrease of left-lateral stress (Figure 12) and was thereby put into a "stress shadow." Such is consistent with the relative locations of the premainshock and postmainshock strike-slip events in the upper plate.

From the above limited coverage of the upper plate seismicity and comparisons with our 3-D models of subduction earthquake cycles with heterogeneous coupling along the interplate interface we conclude that in the majority of cases the location and mode of such seismicity is consistent with space- and time-dependent stressing as predicted by modeling. This confirms earlier observations that seismicity in the vicinity of large/great subduction earthquakes (in the outer rise, at intermediate depth and now in the upper plate) depends on time in the earthquake cycle as well as on coupling patterns along the interplate interface. If such coupling patterns are roughly constant at least from one cycle to another, then the observations of this kind of seismicity could be important in understanding earthquake cycles and, perhaps, in anticipating slip distributions in future subduction events.

References

Astiz, L., T. Lay, and H. Kanamori, Large intermediate depth earthquakes and the subduction process, *Phys. Earth Planet. Inter* 53, 80-166, 1988.

Beck, S.L., and D.H. Christensen, Rupture process of the February 4, 1965, Rat Islands earthquake, *J. Geophys. Res.*, *96*, 2205-2201, 1991.

Boyd, T. M., and J. L. Nábělek, Rupture process of the Andreanof Islands earthquake of May, 1986, *Bull. Seismol. Soc. Am.*, *78*, 1653-1673, 1988.

Chinnery, M. A., Secondary faulting, 1, Theoretical aspects, *Can. J. Earth Sci.*, *3*, 163-174, 1966a.

Chinnery, M. A., Secondary faulting, 2, Geophysical aspects, *Can. J. Earth Sci.*, *3*, 175-190, 1966b.

Christensen, D. H., and L. J. Ruff, Outer-rise earthquakes and seismic coupling, *Geophys. Res. Lett.*, *10*, 697-700, 1983.

Christensen, D. H., and L. J. Ruff, Seismic coupling and outer-rise earthquakes, *J. Geophys. Res.*, *93*, 13421-13444, 1988.

Cormier, V. F., Tectonics near the junction of the Aleutian and Kurile-Kamchatka arcs and a mechanism for Middle-Tertiary magmatism in the Kamchatka Basin, *Geol. Soc. Am. Bull.*, *86*, 443-453, 1975a.

Cormier, V. F., Composite focal mechanism solution of the Near Islands (Aleutian Islands) earthquakes of February 2, 1975 (abstract), *Eos, Trans. AGU*, *56*, 393, 1975b.

Das, S., and B. V. Kostrov, Inversion for seismic slip rate history and distribution with stabilizing constraints: Application to the 1986 Andreanof Islands earthquake, *J. Geophys. Res.*, *95*, 6899-6913, 1990.

Deng, J., and L. R. Sykes, Evolution of the stress field in the southern California and triggering of moderate-size earthquakes: A 200 year perspective, *J. Geophys. Res.*, *102*, 9859-9886, 1997.

Dmowska, R., and L. C. Lovison, Intermediate-term seismic precursors for some coupled subduction zones, *Pure Appl. Geophys.*, *126*, 643-664, 1988.

Dmowska, R., and L. C. Lovison, Influence of asperities along subduction interfaces on the stressing and seismicity of adjacent areas, *Tectonophysics*, *211*, 23-43, 1992.

Dmowska, R., J. R. Rice, L. C. Lovison, and D. Josell, Stress transfer and seismic phenomena in coupled subduction zones during the earthquake cycle, *J. Geophys. Res.*, *93*, 7869-7884, 1988.

Dmowska, R., G. Zheng, and J. R. Rice, Seismicity and deformation at convergent margins due to heterogeneous coupling, *J. Geophys. Res.*, *101*, 3015-3029, 1996a.

Dmowska, R., M. A. J. Taylor, J. R. Rice, and E. A. Okal, Constraining slip heterogeneity of the February 17, 1996 Biak (Mw 8.2), Indonesia, earthquake from pre- and post-event seismicity, *Eos, Trans. AGU*, *77* (17) Spring Meet. Suppl., S184, 1996b.

Ekström, G., and E. R. Engdahl, Earthquake source parameters and stress distribution in the Adak Island region of the central Aleutian Islands, Alaska, *J. Geophys. Res.*, *94*, 15499-15519, 1989.

Engdahl, E. R., S. Billington, and C. Kisslinger, Teleseismically recorded seismicity before and after the May 7, 1986, Andreanof Islands, Alaska, earthquake, *J. Geophys. Res.*, *94*, 15481-15498, 1989.

Geist, E. L., J. R. Childs, and D. W. Scholl, The origin of summit basins of the Aleutian Ridge: Implications for block rotation of an arc massif, *Tectonics*, *7*, 327-342, 1988.

Harris, R. A., and R. W. Simpson, Changes in static stress on southern California faults after the 1992 Landers earthquake, *Nature*, *360*, 251-254, 1992.

Harris, R. A., and r. W. Simpson, suppression of large earthquakes by stress shadows: A comparison of Coulomb and rate-and-state failure, *J. Geophys. Res.*, this issue.

Harris, R. A., and R. W. Simpson, In the shadow of 1857-Effect of the *M*8 Ft. Tejon, California, earthquake on subsequent earthquakes in southern California, *Geophys. Res. Lett.*, *23*, 3, 229-232, 1996.

Harris, R. A., R. W. Simpson, and P. A. Reasenberg, Influence of static stress changes on earthquake locations in southern California, *Nature*, *375*, 221-224, 1995.

Houston, H., and E. R. Engdahl, A comparison of the spatio-temporal distribution of moment release for the Andreanof Islands earthquake with relocated seismicity, *Geophys. Res. Lett.*, *16*, 1421-1424, 1989.

Hubbert, M. K. and W. W. Rubey, Role of fluid pressure in the mechanics of overthrust faulting, *Geol. Soc. Am. Bull.*, *70*, 115-205, 1959.

Hwang, L. J., and H. Kanamori, Source parameters of the May 7, 1986 Andreanof Islands earthquake, *Geophys. Res. Lett.*, *13*, 1426-1429, 1986.

Jaumé, S. C., and L. R. Sykes, Change in the state of stress on the southern San Andreas fault resulting from the California earthquake sequence of April to June 1992, *Science*, *258*, 1325-1328, 1992.

King, G. C. P., R. S. Stein, and J. Lin, Static stress changes and the triggering of earthquakes, *Bull. Seismol. Soc. Am.*, *84*, 935-953, 1994.

Lay, T., L. Astiz, H. Kanamori, and D. H. Christensen, Temporal variation of large interplate earthquakes in coupled subduction zones, *Phys. Earth Planet. Inter.*, *54*, 258-312, 1989.

Minster, J. B., and T. H. Jordan, Present-day plate motions, *J. Geophys. Res.*, *83*, 5331-5354, 1978.

Newberry, J. T., D. L. Laclair, and K. Fujita, Seismicity and tectonics of the far western Aleutian Islands, *J. Geodyn.*, *6*, 13-32, 1986.

Puntodewo, S. S. O., R. McCaffrey, E. Calais, Y. Bock, J. Rais, C. Subarya, R. Poewariardi, C. Stevens, J. Genrich, Fauzi, P. Zwick, and S. Wdowinski, GPS measurements of crustal deformation within the Pacific-Australia plate boundary zone in Irian Jaya, Indonesia, *Tectonophysics*, *237*, 141-153, 1994.

Rayleigh, C. B., J. H. Healy, and J. D. Bredehoeft, Faulting and crustal stress at Rangely, Colorado, in *Flow and Fracture of Rocks, Geophys. Monogr. Ser.*, vol 16, edited by H. C. Heard et al., pp. 275-284, AGU, Washington, D.C., 1972.

Reasenberg, P. A., and R. W. Simpson, Response of regional seismicity to the static stress change produced by the Loma Prieta earthquake, *Science*, *255*, 1687-1690, 1992.

Rybicki, K., Dependence of the spatial distribution of aftershocks on the site of the dislocation area at the time of the main earthquake, *Publ. Inst. Geophys. Pol. Acad. Sci.*, *36*, 117-126, 1970.

Rybicki, K., Analysis of aftershocks on the basis of dislocation theory, *Phys. Earth Planet. Inter.*, *7*, 409-422, 1973.

Rybicki, K., T. Kato, and K. Kasahara, Mechanical interaction between neighboring active faults - static and dynamic stress field induced by faulting, *Bull. Earthquake Res. Inst. Univ. Tokyo*, *60*, 1-21, 1985.

Simpson, R. W., and P. A. Reasenberg, Earthquake-induced static-stress changes on central California faults, *U. S. Geological Survey Prof. Pap. 1550-F*, F55-F89, 1994.

Smith, S. W., and W. Van de Lindt, Strain adjustments associated with earthquakes in southern California, *Bull. Seismol. Soc. Am.*, *59*, 1569-1589, 1969.

Stauder, W., Tensional character of earthquake foci beneath the Aleutian trench with relation to sea floor spreading, *J. Geophys. Res.*, *73*, 7693-7701, 1968a.

Stauder, W., Mechanism of the Rat Island earthquake sequence of February 4, 1965, with relation to island arcs and sea-floor spreading, *J. Geophys. Res.*, *73*, 3847-3858, 1968b.

Stein, R. S. and M. Lisowski, The 1979 Homestead Valley earthquake sequence, California: Control of aftershocks and postseismic deformation, *J. Geophys. Res.*, *88*, 6477-6490, 1983.

Stein, R. S., G. C. P. King, and J. Lin, Change in failure stress on the southern San Andreas fault system caused by the 1992 magnitude = 7.4 Landers earthquake, *Science*, *258*, 1328-1332, 1992.

Taylor, M. A. J., G. Zheng, J. R. Rice, W. D. Stuart, and R. Dmowska, Cyclic stressing and seismicity at strongly coupled subduction zones, *J. Geophys. Res.*, *101*, 8363-8381, 1996.

Wu, F. T., and H. Kanamori, Source mechanism of February 4, 1965, Rat Island earthquake, *J. Geophys. Res.*, *78*, 6082-6092, 1973.

Yoshida, S., Waveform inversion for rupture process using a non-flat seafloor model: Application to 1986 Andreanof Islands and 1985 Chile earthquakes, *Tectonophysics*, *211*, 45-59, 1992.

Yu, G., S. G. Wesnousky, and G. Ekström, Slip partitioning along major convergent plate boundaries, *Pure Appl. Geophys.*, *140*, 183-210, 1993.

Zheng, G., R. Dmowska, and J. R. Rice, Modeling earthquake cycles in the Shumagins subduction segment, Alaska, with seismic and geodetic constraints, *J. Geophys. Res.*, *101*, 8383-8392, 1996.

R. Dmowska, J. R. Rice, and M. A. J. Taylor, Division of Engineering and Applied Sciences, Harvard University, 327 Pierce Hall, 29 Oxford Street, Cambridge, MA 02138. (e-mail: taylor@esag.harvard.edu)